Appendix A. Supplementary data

Supplementary data associated with this article can be found, in the online version, at doi:10.1016/j.jconrel.2006.07.014.

References

[1] M.A. Kay, D.X. Liu, P.M. Hoogerbrugge, Gene therapy, Proc. Natl. Acad. Sci. 88 (1997) 5572–5576.

[2] I.M. Verma, N. Somia, Gene therapy—promises, problems and prospects, Nature 389 (1997) 239–242.

[3] W.F. Anderson, Human gene therapy, Nature 392 (1998) 25–30.

[4] D. Luo, W.M. Saltzman, Synthetic DNA delivery system, Nature 18 (2000) 33–37.

[5] O. Boussif, F. Lezoualc'h, M.A. Zanta, M.D. Mergny, D. Scherman, B. Demeneix, J.P. Behr, Versatile vector for gene and oligonucleotide transfer into cells in culture and in vivo: polyethylenimine, Proc. Natl. Acad. Sci. 92 (1995) 7297–7301.

[6] B. Abdallah, A. Hassan, C. Benoist, D. Goula, J.P. Behr, B.A. Demeneix, A powerful non-viral vector for in vivo gene transfer into the adult mammalian brain: polyethilenimine, Hum. Gene Ther. 7 (1996) 1947–1954.

[7] D. Fischer, T. Bieber, Y. Li, H.P. Elsasser, T. Kissel, A novel non viral vector for DNA delivery based on low molecular weight, branched polythylenimine: effect of molecular weight on transfection efficiency and cytotoxicity, Pharm. Res. 16 (1999) 1273–1279.

[8] S. Boeckle, K. von Gersdorff, S. van der Piepen, C. Culmsee, E. Wagner, M. Ogris, Purification of polyethylenimine polyplexes highlights the role of free polycations in gene transfer, J. Gene Med. 6 (2004) 1102–1111.

[9] P.K. Selbo, A. Hogste, L. Prasmickaite, K. Berg, Photochemical internalization: a novel drug delivery system, Tumor Biol. 23 (2002) 103–112.

[10] K. Berg, P.K. Selbo, L. Prasmickaite, T. Tjelle, K. Sandvig, J. Moan, G. Gaudernack, O. Fodstad, S. Kjolsrud, H. Anholt, G.H. Rodal, S. Rodal, A. Høgset, Photochemical internalization : a novel technology for delivery of macromolecules into cytosol, Cancer Res. 59 (1999) 1180–1183.

[11] A. Høgset, L. Prasmickaite, T.E. Tjelle, K. Berg, Photochemical transfection: a new technology for light-induced, site-directed gene delivery, Hum. Gene Ther. 11 (2000) 869–880.

[12] A. Høgset, L. Prasmickaite, P.K. Selbo, M. Hellum, B.Ø. Engesæter, A. Bondted, K. Berg, Photochemical internalization in drug and gene delivery, Adv. Drug Deliv. Rev. 56 (2004) 95–115.

[13] I.J. Macdonald, T.J. Dougherty, Basic principle of photodynamic therapy, J. Porphyr. Phthalocyanines 5 (2001) 105–129.

[14] N. Nishiyama, A. Iriyama, W.-D. Jang, K. Miyata, K. Itaka, Y. Inoue, H. Takahashi, Y. Yanagi, Y. Tamaki, H. Koyama, K. Kataoka, Light induced gene transfer from packaged enveloped in a dendrimeric photosensitizer, Nat. Matters 4 (2005) 934–941.

[15] Y. Takakura, H. Hashida, Macromolecular carrier systems for targeted drug delivery: pharmacokinetic considerations on biodistribution, Pharm. Res. 13 (1996) 820–831.

[16] K. Itaka, K. Yamauchi, A. Harada, K. Nakamura, H. Kawaguchi, K. Kataoka, Polyion complex micelles from plasmid DNA and poly(ethylene glycol)-poly(L-lysine) block copolymer as serum-tolerable polyplex system: physicochemical properties of micelles relevant to gene transfection efficiency, Biomaterials 24 (2003) 4495–4506.

[17] M. Harada-Shiba, K. Yamauchi, A. Harada, K. Shimokado, K. Kataoka, Polyion complex micelles as a vector for gene therapy-pharmacokinetics and in vivo gene transfer, Gene Ther. 9 (2002) 407–414.

[18] K. Miyata, Y. Kakizawa, N. Nishiyama, A. Harada, Y. Yamasaki, H. Koyama, K. Kataoka, Block catiomer polyplexes with regulated densities of charge and disulfide cross-linking directed enhance gene expression, J. Am. Chem. Soc. 126 (2004) 2355–2361.

[19] N. Nishiyama, Arnida, W.-D. Jang, K. Date, K. Miyata, K. Kataoka, Photochemical enhancement of transgene expression by polymeric micelles incorporating plasmid DNA and dendrimer-based photosensitizer, J. Drug Target 14 (2006) 413–424.

[20] N. Kanayama, N. Nishiyama, S. Fukushima, K. Itaka, W.-D. Jang, K. Miyata, Y. Yamasaki, K. Kataoka, PEG-based biocompatible block catiomer with high-buffering capacity for the construction of polyplex micelles showing efficient gene transfer toward primary cells, ChemMedChem 1 (2006) 439–444.

[21] A.C.H. Ng, X. Li, D.K.P. Ng, Synthesis and photophysical properties of non-aggregated phthalocyanines bearing dendritic substitutes, Macromolecules 32 (1999) 5292–5298.

[22] W.-D. Jang, Y. Nakagishi, N. Nishiyama, S. Kawauchi, Y. Morimoto, M. Kikuchi, K. Kataoka, Polyion complex micelle for photodynamic therapy: incorporation of dendritic photosensitizer excitable at long wavelength with enhanced cellular uptake, J. Control. Rel. 113 (2006) 73–79.

[23] H. Niwa, K. Yamamura, J. Miyazaki, Efficient selection for high-expression transfectants with a novel eukaryotic vector, Gene 108 (1991) 193–199.

[24] A. Harada, K. Kataoka, Formation of polyion polyplex micelles in aqueous milieu from a pair of oppositely-charged block copolymers with poly (ethylene glycol) segment, Macromolecules 285 (1995) 294–5299.

[25] M.B. Hansen, S.E. Nielsen, K. Berg, Re-examination and further development of a precise and rapid dye method for measuring cell growth/cell kill, J. Immunol. Methods 119 (1989) 203–210.

[26] K. Itaka, A. Harada, K. Nakamura, H. Kawaguchi, K. Kataoka, Evaluation by fluorescence resonance energy transfer of the stability of non viral gene delivery vectors under physiological conditions, Biomacromolecules 3 (2002) 841–845.

[27] J.S. Zhang, F. Liu, L. Huang, Implication of pharmacokinetic behavior of lipoplex for its inflammatory cytotoxicity, Adv. Drug Deliv. Rev. 57 (2005) 689–698.

[28] R.K. Jain, D. Fukumura, D.E.J.G.J. Dolmans, Photodynamic therapy for cancer, Nat. Rev., Cancer 3 (2003) 380–387.

[29] Y. Bae, N. Nishiyama, S. Fukushima, H. Koyama, Y. Matsumura, K. Kataoka, Preparation and biological characterization of polymeric micelle drug carriers with intracellular pH-triggered drug release property: tumor permeability, controlled subcellular drug distribution, and enhanced *in vivo* antitumor efficacy, Bioconjug. Chem. 16 (2005) 122–130.

[30] N. Nishiyama, S. Okazaki, H. Cabral, M. Miyamoto, Y. Kato, Y. Sugiyama, K. Nishio, Y. Matsumura, K. Kataoka, Novel cisplatin-incorporated polymeric micelles can eradicate solid tumors in mice, Cancer Res. 63 (2003) 8977–8983.

[31] J. Moan, K. Berg, A. Anholt, K. Madslien, Sulfonated aluminum phthalocyanines as sensitizers for photochemotherapy. Effects of small doses on localization, dye fluorescence and photosensitivity in V79 cells, Int. J. Cancer 58 (1994) 865–870.

Precise Control of Lower Critical Solution Temperature of Thermosensitive Poly(2-isopropyl-2-oxazoline) via Gradient Copolymerization with 2-Ethyl-2-oxazoline as a Hydrophilic Comonomer

Joon-Sik Park[†] and Kazunori Kataoka*[,†,‡,§]

Department of Materials Engineering, Graduate School of Engineering, The University of Tokyo, 7-3-1 Hongo, Bunkyo-ku, Tokyo 113-8656, Japan; Center for Disease Biology and Integrative Medicine, Graduate School of Medicine, The University of Tokyo, Tokyo 113-0033, Japan; and Center for NanoBio Integration, The University of Tokyo, 7-3-1 Hongo, Bunkyo-ku, Tokyo 113-8656, Japan

Received March 13, 2006; Revised Manuscript Received June 23, 2006

ABSTRACT: The lower critical solution temperature (LCST) of amphiphilic poly(2-isopropyl-2-oxazoline) (P*i*PrOx) was precisely tuned via the copolymerization with 2-ethyl-2-oxazoline (EtOx) as a hydrophilic comonomer. The copolymerization was cationically initiated by methyl *p*-tosylate at the optimum condition (42 °C in acetonitrile) for living polymerization, obtaining the copolymers with a narrow molecular weight distribution ($M_w/M_n \leq 1.02$). The monomer reactivity ratios of 1.78 and 0.79 respectively were derived for EtOx and *i*PrOx from the cumulative and instantaneous compositions of the copolymers determined from the ^{1}H NMR and MALDI-TOF mass spectrometry. This set of the reactivity ratios are sufficiently different enough to form the gradient copolymers, in which each polymer chain has a trend of a gradually decreasing EtOx and an increasing *i*PrOx composition along the backbone from the α-terminal to ω-chain end. These gradient copolymers followed a rather simple rule in their thermosensitive behaviors to show a linear increase in LCST with an increasing mol % of EtOx. Consequently, a series of P(EtOx-*co*-*i*PrOx) with finely tuned LCST in aqueous medium were obtained through the cationic copolymerization simply by varying the initial composition of both monomers, opening a new way to engineer the thermosensitivity of polymeric materials directing to particular applications.

Introduction

Recently, enormous attention has been paid to so-called "smart" polymeric materials showing a discrete change in their propensity responding to external physical and chemical stimuli, including light, temperature, pH, and magnetic and electric fields. Of special interest is temperature-responsive polymers useful for various practical applications, such as supports for catalysts,[1] sensors,[2] separation systems,[3] enzymatic bioconjugates,[4] and drug carriers.[5] Drastic changes in solubility, turbidity, and other physicochemical properties of thermosensitive polymers can be simply induced by adding or removing heat energy, and such feasibility is particularly important to design "smart" polymeric materials that instantly respond to the external stimuli. Careful engineering of polymer structure should be needed for the fine-tuning of responding temperature as well as sharpness of transition. Furthermore, additional functionalization in a controllable manner may be required for some applications directing to construct thermosensitive block or graft copolymers, which have received growing interest particularly in bio-related fields.

In this regard, we have been recently focusing on the quantitative polymerization and selective end-functionalization of thermosensitive poly(2-isopropyl-2-oxazoline) (P*i*PrOx) telechelics.[6] The polymerization proceeded in a good controlled manner under an optimum temperature condition (42 °C) with appreciably narrow molecular weight distributions ($M_w/M_n \leq$ 1.03), having never been accomplished in those of the conventional poly(2-oxazolines) (POx) homologues often viewed as "pseudopeptides".[7] Of importance is that P*i*PrOx exhibits a characteristic lower critical solution temperature (LCST) near physiological conditions, like poly(*N*-isopropylacrylamide) (PNIPAAm),[8] the typical representative of the thermosensitive polymers with numerous applications. The notable transition behaviors of P*i*PrOx, characterized by a fast responsivity, viz., transition sharpness, could be achieved by the precise control of the well-defined polymeric structures through the living polymerization mechanism. It should be also noted that POx, as a rule, are nontoxic and that some of them carry US Food and Drug Administration (FDA) approval.[9]

In the meantime, the LCST of P*i*PrOx can be controlled by incorporating the specific composition of hydrophilic or hydrophobic 2-oxazoline monomer units within the main chains, as in the case of conventional thermosensitive polymers.[10] A number of recent studies have shown that thermosensitive copolymers from different monomers are simply synthesized by the living ionic or controlled/living radical polymerization technique, and these copolymers with well-balanced hydrophilic/hydrophobic monomer sequences are attractive to realize the elaborate manipulability of their LCST values.[11] Nevertheless, little attention has been paid to the living cationic copolymerization between 2-isopropyl-2-oxazoline (*i*PrOx) and various hydrophilic/hydrophobic 2-substituted-2-oxazolines (Ox). Although there are several examples of copolymers composed of some Ox sequences including *i*PrOx,[12] the study on the LCST control of POx through the well-defined cationic copolymerization of *i*PrOx with either the hydrophilic or hydrophobic Ox comonomer has not been accomplished yet. Because there are various hydrophilic and hydrophobic Ox monomers, it is

† Graduate School of Engineering.
‡ Graduate School of Medicine.
§ Center for NanoBio Integration.
* To whom correspondence should be addressed: Tel +81-3-5841-7138; Fax +81-3-5841-7139; e-mail kataoka@bmw.t.u-tokyo.ac.jp.

10.1021/ma0605548 CCC: $33.50
Published on Web 08/22/2006

Scheme 1. Synthetic Scheme for the Gradient Copolymerization of 2-Ethyl-2-oxazoline (EtOx) and 2-Isopropyl-2-oxazoline (*i*PrOx) Initiated with Methyl *p*-Tosylate

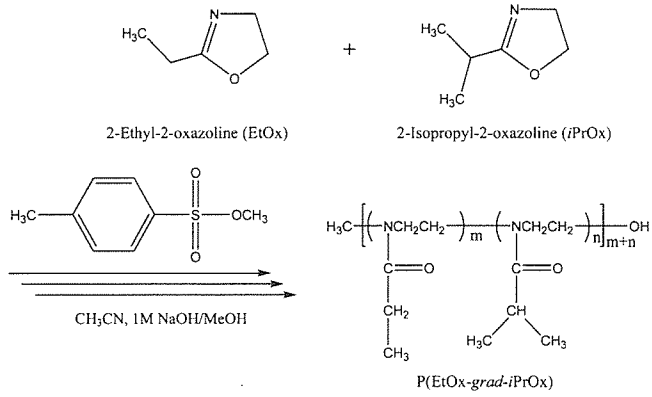

relatively easy to select the appropriate comonomer for varying the solubility of P*i*PrOx in water. However, careful consideration should also be taken into account for the diversity of the copolymerization conditions, derived from the many combinations among initiators, solvents, and temperatures vs the respective Ox monomers. It has been also noted that, in the controlled living copolymerization system of two monomers with sufficiently different reactivity ratios, a gradient copolymer, in which the instantaneous composition continuously varies along the chain contour, could be predominantly produced due to the feed composition drift that spontaneously occurs during the reaction.[13] Therefore, it was hypothesized that the choice of the appropriate hydrophilic or hydrophobic Ox comonomer exhibiting a sufficiently different reactivity against the *i*PrOx monomer may create thermosensitive gradient copolymers.

In the present study, we report the facile and precise synthetic route of thermosensitive gradient copolymers via the living cationic polymerization of *i*PrOx, including the specific composition of EtOx as a hydrophilic comonomer (Scheme 1). It was confirmed from the ^{1}H NMR and MALDI-TOF mass spectrometry that EtOx and *i*PrOx were found to have reactivity ratios sufficiently different from gradient copolymers under mild temperature conditions (42 °C). Furthermore, these POx gradient copolymers showed a rapid and linear response to temperature change from 38.7 to 67.3 °C.

Experimental Section

Materials. 2-Isopropyl-2-oxaxoline was synthesized from isobutyric acid (Wako Pure Chemical Industries, Ltd., Osaka, Japan) and 2-aminoethanol (Wako Pure Chemical Industries) as previously described.[6,14] Methyl *p*-tosylate (Tokyo Kasei Kogyo Co., Ltd., Tokyo, Japan) was distilled from calcium hydride under reduced pressure. 2-Ethyl-2-oxaxoline (Aldrich Chemical Co., Ltd., Milwaukee, WI) and acetonitrile (Wako Pure Chemical Industries) were distilled from calcium hydride following conventional procedures.[15] Other chemicals such as the 1 N NaOH aqueous solution and methanol were purchased from Wako Pure Chemical Industries and used without further purification.

Techniques. The ^{1}H NMR spectra were recorded using a JEOL EX 300 spectrometer at 300 MHz. The chemical shifts were reported in parts per million (ppm) downfield from tetramethylsilane. The molecular weights and molecular weight distributions were determined using a GPC (TOSOH HLC-8220) system equipped with two TSK gel columns (G4000H$_{HR}$ and G3000H$_{HR}$) and an internal refractive index (RI) detector. The columns were eluted with DMF containing lithium bromide (10 mM) and triethylamine (30 mM) at the flow rate of 0.8 mL/min and were maintained at a temperature of 40 °C. The molecular weights were calibrated using poly(ethylene glycol) (PEG) standards (Polymer Laboratories, Ltd., UK). The mass measurements were performed using a MALDI-TOF mass spectrometer (Bruker REFLEX III), operating at an acceleration voltage of 23 kV in the reflection mode. The UV−vis spectra were obtained using a V-550 UV/vis JASCO spectrophotometer.

Synthesis of Poly(2-isopropyl-2-oxazoline) (P*i*PrOx) Having a Hydroxyl Group at the ω-Terminal End. 2-Isopropyl-2-oxazoline (*i*PrOx) (10 g, 88.4 mmol) was added via a syringe to a solution of methyl *p*-tosylate (MeOTs) (0.186 g, 1.0 mmol) in acetonitrile (30 mL). The polymerization mixture was stirred at 42 °C for 476.5 h under an argon atmosphere. The mixture was cooled to room temperature and treated with methanolic NaOH (1 M) to introduce a hydroxyl group at one of the chain ends. The solution of Me-P*i*PrOx-OH was purified via dialysis for 2 days against distilled water and then recovered by lyophilization. Six samples were collected during the course of the polymerization. They were subjected to the same treatment above and analyzed by a MALDI-TOF mass spectrometer in order to determine the conversion yield (total yields: 9 g, 90%).

Synthesis of Poly(2-ethyl-2-oxazoline) (PEtOx) Having a Hydroxyl Group at the ω-Terminal End. 2-Ethyl-2-oxazoline (EtOx) (8.763 g, 88.4 mmol) was added via a syringe to a solution of MeOTs (0.186 g, 1.0 mmol) in acetonitrile (30 mL). The polymerization mixture was stirred at 42 °C for 315 h under an argon atmosphere. The mixture was then cooled to room temperature and treated with methanolic NaOH (1 M) to introduce a hydroxyl group at one of the chain ends. The solution of Me-PEtOx-OH was purified via dialysis for 2 days against distilled water and then recovered by lyophilization. Four samples were collected during the course of the polymerization. They were subjected to the same treatment described above and analyzed using a MALDI-TOF mass spectrometer in order to determine the conversion yield (total yields: 8.3 g, 95%).

Synthesis of Gradient Copolymers (P(EtOx$_{25\%}$*i*PrOx$_{75\%}$), P(EtOx$_{50\%}$*i*PrOx$_{50\%}$), P(EtOx$_{75\%}$*i*PrOx$_{25\%}$)) Having a Hydroxyl Group at the ω-Terminal End. The respective mixtures of 2-ethyl-2-oxazoline (EtOx$_{25\%}$: 2.19 g, 22.1 mmol; EtOx$_{50\%}$: 4.38 g, 44.2 mmol; EtOx$_{75\%}$: 6.57 g, 66.3 mmol) and 2-isopropyl-2-oxazoline (*i*PrOx$_{75\%}$: 7.5 g, 66.3 mmol; *i*PrOx$_{50\%}$: 5 g, 44.2 mmol; *i*PrOx$_{25\%}$: 2.5 g, 22.1 mmol) were added to a solution of MeOTs (0.186 g, 1.0 mmol) in acetonitrile (30 mL). The polymerization mixture was stirred at 42 °C for 309.5 h (P(EtOx$_{25\%}$*i*PrOx$_{75\%}$)), 407 h (P(EtOx$_{50\%}$*i*PrOx$_{50\%}$)), and 288 h (P(EtOx$_{75\%}$*i*PrOx$_{25\%}$)) under an argon atmosphere. The reaction mixtures were cooled to room temperature and then treated with methanolic NaOH (1 M) to introduce a hydroxyl group at one of the chain ends. The copolymer solutions were purified via dialysis for 2 days against distilled water and then recovered by lyophilization. Several samples of the respective copolymers were collected during the course of the copolymerization. They were subjected to the same treatment as described above and analyzed by MALDI-TOF mass and ^{1}H NMR spectrometers in order to determine the conversion yield and composition of the copolymers (total yields: 8.4 g, 87% (P(EtOx$_{25\%}$*i*PrOx$_{75\%}$)), 8.5 g, 91% (P(EtOx$_{50\%}$*i*PrOx$_{50\%}$)), 7.7 g, 85% (P(EtOx$_{75\%}$*i*PrOx$_{25\%}$)).

MALDI-TOF Mass Spectrometry. An external calibration was performed using poly(ethylene glycol) standards (MeO-PEG-OH; MW = 5000, 12 000, NOF Corp). Ions were generated by laser desorption at 337 nm (N_2 laser, 3 ns pulse width, 10^6−10^7 W/cm^2). For each spectrum, ~400 transients were accumulated and all spectra were recorded in the reflection mode. The data evaluation was performed with the Bruker XMASS program using the reflection spectra only in order to achieve a better signal-to-noise ratio. α-Cyano-4-hydroxycinnamic acid (CCA) (Fluka) was selected as a suitable matrix. A trifluoroacetic acid/acetonitrile (0.1% TFA: CH_3CN = 2:1) solution of CCA (10 mg/mL) was mixed with a solution of the polymer in acetonitrile (1 mg/mL) at an equimolar ratio. The resulting mixture was shaken for a few seconds. An aliquot of the mixture (1 μL) was placed on the target plate and inserted into the ion source chamber after being slowly dried. The polymer concentration of the polymer/matrix mixture solution could

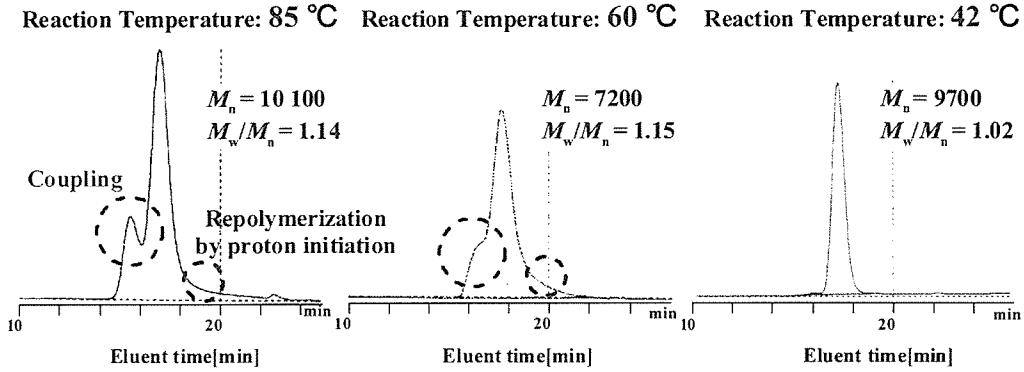

Figure 1. GPC diagrams of P*i*PrOx (DP_{theo} = 88.4) synthesized under different temperature conditions (PEG standard, eluent: DMF (containing 10 mM LiCl and 30 mM TEA), temperature: 40 °C, RI detection).

Table 1. Copolymerization Results of *i*PrOx with EtOx at Different Feed Composition[a] and Their T_{cp} Values

feed ratio (EtOx:*i*PrOx)	yield (%)	M_n (M_w/M_n) MALDI-TOF-MS[b]	M_n (M_w/M_n) GPC[c]	*m*:*n*[d]	T_{cp}[e] (°C) (with 150 mM NaCl)
100:0	95	8300 (1.01)	8000 (1.02)	100:0	
25:75	87	8700 (1.01)	9300 (1.02)	22:78	67.3 (65.4)
50:50	91	9300 (1.01)	9300 (1.02)	48:52	55.2 (54.0)
75:25	85	9100 (1.01)	9300 (1.02)	73:27	46.0 (45.1)
0:100	90	10200 (1.01)	9700 (1.02)	0:100	38.7 (37.4)

[a] Reaction conditions: ([EtOx] + [*i*PrOx])/$[MeOTs]_{init}$ = 88.4, $[MeOTs]_{init}/[CH_3CN]_{solv}$ = 0.033 mol/L, 42 °C, terminated with methanolic NaOH (1 M) for hydroxyl ω-end group. [b] Bruker REFLEX III, operating at an acceleration voltage of 23 kV in the reflector mode. [c] DMF (10 mM LiCl and 30 mM TEA), 40 °C, RI detection. [d] Determined by ^{1}H NMR spectroscopy for the final copolymer products (monomer composition: *m* = [EtOx], *n* = [*i*PrOx]). [e] Measured by UV−vis spectroscopy (*c* = 1.0 wt %).

be diluted for the optimum ionization with an acetone solution of CCA (10 mg/mL).

Turbidity Measurements. Cloud points were determined by spectrophotometric detection of the changes in transmittance (λ = 500 nm) of the aqueous polymer solutions (1.0 wt %) heated at a constant rate (0.5 °C/min). The samples were placed in a temperature-controlled circulating water bath. Values for the cloud points of the polymer solutions were determined as the temperature corresponding to a 10% decrease in optical transmittance.

Results and Discussion

Synthesis of Homopolymers. Prior to the synthesis of copolymers, the respective polymerization behaviors of both the P*i*PrOx and PEtOx homopolymers needed to be screened in order to gain the kinetic information under the identical reaction conditions.

As far as the polymerization of *i*PrOx initiated with methyl *p*-tosylate (MeOTs) in acetonitrile, the mild temperature condition should be adapted for avoiding the spontaneously occurring side reactions such as chain transfer and coupling, resulting in wide molecular weight distributions (Figure 1). There has been an argument that the branching in 2-alkyl-2-oxazoline polymerization is susceptible to occur with the increasing monomer conversion, deriving from a chain transfer to monomer followed by repolymerization and coupling.[16] This effect was visible in the GPC traces of Figure 1 as a lower molecular weight tailing and a higher molecular weight shoulder, even notable with increasing temperature. In particular, at polymerization temperature of 85 °C, the higher molecular weight shoulder on the GPC diagram become pronounced, which is most likely due to the occurrence of a coupling or branching. In the chain transfer step, a monomer, instead of adding nucleophilically to the growing chain end, abstracts a proton to produce a dormant enamine-terminated polymer chain and an oxazolinium monomer which can continue the kinetic chain. In the coupling (or branching) step, after the majority of the presumably more

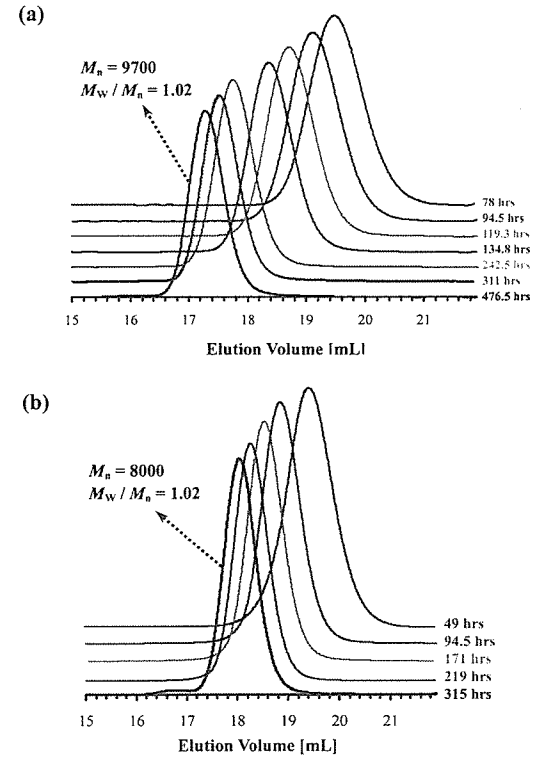

Figure 2. GPC traces of two homopolymers ((a) P*i*PrOx and (b) PEtOx) having different molecular weights (PEG standard, eluent: DMF (containing 10 mM LiCl and 30 mM TEA), temperature: 40 °C, RI detection).

reactive oxazoline monomer is exhausted, the terminal enamine end groups on the dormant chains are able to compete for the oxazolinium chain ends. Each of these couplings produces a branch point and regenerates another oxazolinium end group. The evidence of these side reactions was often observed as both lower molecular weight tailings and higher molecular weight shoulders in the GPC traces of P*i*PrOx, so that the mild

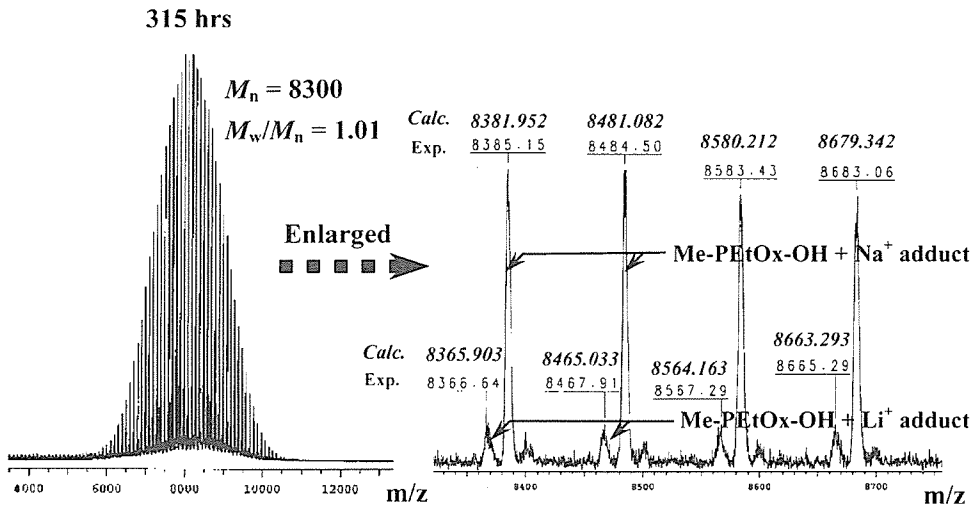

Figure 3. MALDI-TOF mass spectrum of ω-hydroxyl-terminated PEtOx after 315 h (left) and its expanded spectrum in the region of 8330−8750 (right).

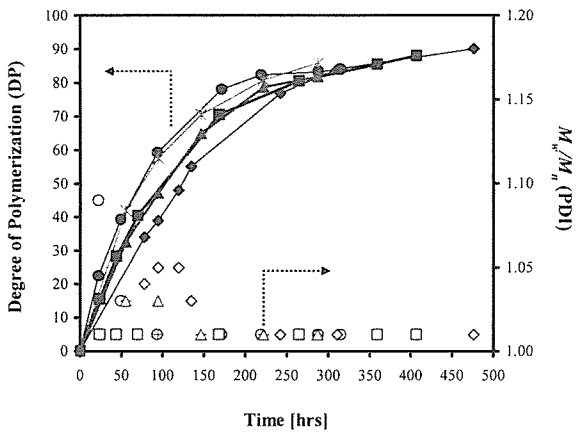

Figure 4. Degree of polymerization (DP) (closed symbols) and polydispersity index (PDI) (open symbols), obtained from MALDI-TOF mass spectrometry, against reaction time for two homopolymers (P*i*PrOx (◆, ◇) and PEtOx (●, ○)) and three gradient copolymers (P(EtOx$_{25\%}$*i*PrOx$_{75\%}$) (▲, △), P(EtOx$_{50\%}$*i*PrOx$_{50\%}$) (■, □), and P(EtOx$_{75\%}$*i*PrOx$_{25\%}$) (*, +)).

temperature of 42 °C was found to be a key condition factor to have complete control over the side reactions (Figure 1).

Based on the results described above, the cationic ring-opening polymerization of *i*PrOx initiated with MeOTs was done to obtain the well-defined poly(2-isopropyl-2-oxazoline) carrying a hydroxyl group at one end (Me-P*i*PrOx-OH). Under mild temperature conditions (42 °C), the polymerization had to be left to proceed for lengths of time up to ca. 476.5 h, but no noticeable side reactions occurred. It was ascertained from the GPC diagrams (Figure 2a) and MALDI-TOF mass spectra (Figure S1a−g in the Supporting Information) that the time-dependent change in the number-average molecular weight (M_n) and the molecular weight distribution were consistent with the living polymerization process; the polydispersity index was low (PDI $_{GPC}$ = 1.02, PDI $_{TOF-MS}$ = 1.01), and the experimental M_n value ($M_{n,GPC}$ = 9700, $M_{n,TOF-MS}$ = 10 200) was close to the value predicted from the initial monomer/initiator ratio ($M_{n,calc}$ = 10 000) (Table 1). An end-group analysis of the polymer was also performed from the MALDI-TOF mass spectrum recorded for a Me-P*i*PrOx-OH after 476.5 h (Figure S1g in the Supporting Information). The most intense signal can be assigned to the sodium adduct of Me-P*i*PrOx-OH, while the second most intense signal is due to the potassium adduct of Me-P*i*PrOx-OH.

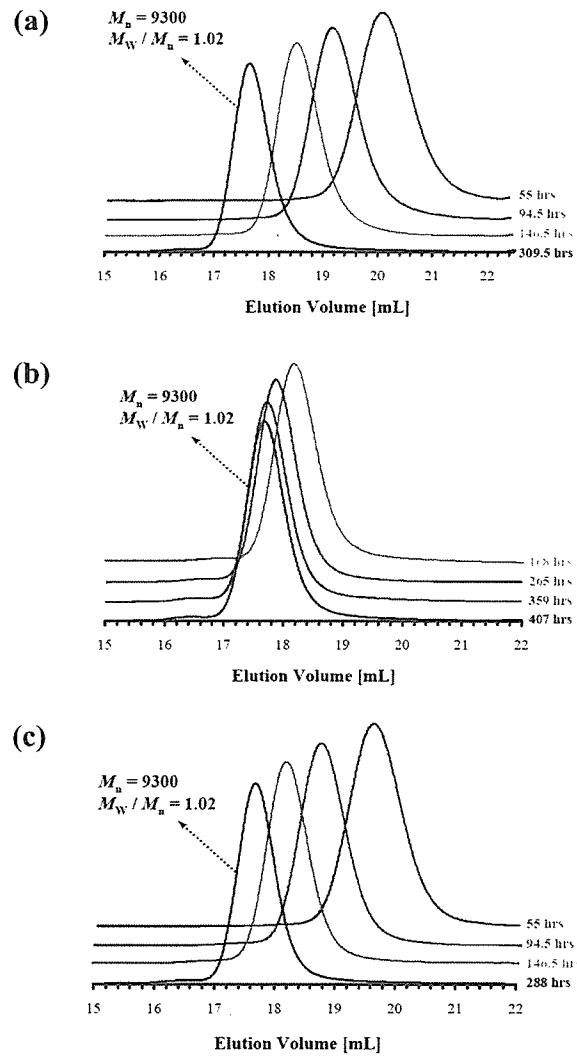

Figure 5. GPC traces of three gradient copolymers ((a) P(EtOx$_{25\%}$*i*PrOx$_{75\%}$), (b) P(EtOx$_{50\%}$*i*PrOx$_{50\%}$), and (c) P(EtOx$_{75\%}$*i*PrOx$_{25\%}$)) having different molecular weights (PEG standard, eluent: DMF (containing 10 mM LiCl and 30 mM TEA), temperature: 40 °C, RI detection).

The polymerization of Me-PEtOx-OH (8.763 g, 88.4 mmol) was also done under the synthetic conditions similar to that of Me-P*i*PrOx-OH with the initiation of methyl *p*-tosylate (MeOTs) (0.186 g, 1.0 mmol) in acetonitrile (30 mL) under mild temperature conditions (42 °C), followed by the treatment with

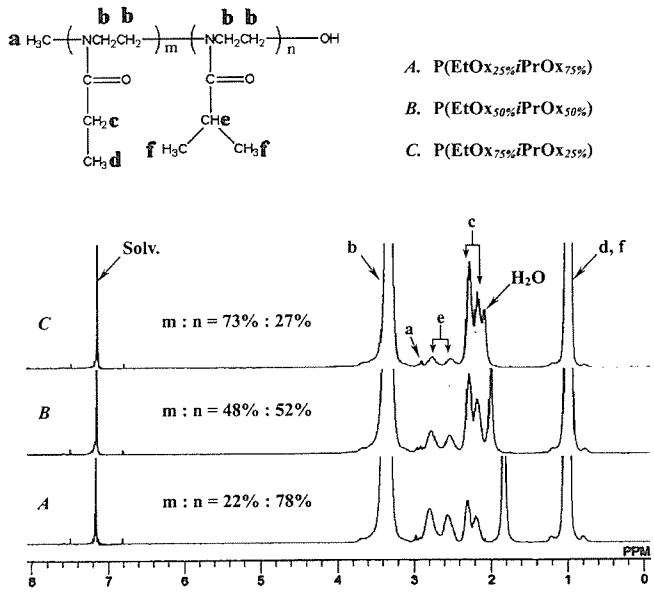

Figure 6. ^{1}H NMR spectra for the final products of three gradient copolymers (P(EtOx$_{25\%}$*i*PrOx$_{75\%}$), P(EtOx$_{50\%}$*i*PrOx$_{50\%}$), and P(EtOx$_{75\%}$*i*PrOx$_{25\%}$)) in $CDCl_3$ at 25 °C.

methanolic NaOH (1 M) for introducing a hydroxyl ω-end group. Under this condition, the polymerization should be left to proceed for ca. 315 h, but no noticeable side reactions occurred, as in the system of Me-P*i*PrOx-OH. It was confirmed from the GPC diagrams (Figure 2b) and MALDI-TOF mass spectra (Figure S2a–d) in the Supporting Information and Figure 3) that the polydispersity indices of all the sampling polymers including the final product were below 1.03, and the experimental M_n value ($M_{n,GPC}$ = 8000, $M_{n,TOF-MS}$ = 8300) was almost identical to the value predicted from the initial monomer/initiator ratio ($M_{n,calc}$ = 8800) (Table 1). The end-group analysis of the Me-PEtOx-OH was also done using the MALDI-TOF mass spectrum recorded after 315 h (Figure 3). The most intense signal can be assigned to the sodium adduct of Me-PEtOx-OH, while the second most intense signal is due to the lithium adduct of Me-PEtOx-OH. The ^{1}H NMR spectrum of Me-PEtOx-OH in $CDCl_3$ presented a broad singlet at 3.4 ppm attributed to the methylene protons of the polymer backbone, two broad singlets at 2.1–2.4 ppm, ascribed to methylene protons of the ethyl side chain and a broad singlet at 1.0 ppm due to the side chain methyl protons (Figure S3). To the best of our knowledge, this is the first demonstration of polymerizing an extremely monodispersive PEtOx homopolymers ($M_w/M_n \leq 1.02$) without inadvertent side reactions such as chain transfer and coupling,[16] often observed during the synthesis of conventional PEtOx systems under high-temperature conditions.[17]

The time-dependent monomer conversion obtained from the MALDI-TOF mass spectrometry for the respective polymerizations of both *i*PrOx and EtOx is also depicted in Figure 4, whereby the degree of polymerization (DP) was positioned at the left ordinate and the polydispersity index (PDI) (M_w/M_n) at the right ordinate. From the time-dependent DP and PDI changes of the two respective homopolymers, it was obvious that the polymerization rate of EtOx (●) was somewhat faster than that of *i*PrOx (◆) at 42 °C.

Synthesis of Gradient Copolymers. In view of the synthesis result of the two homopolymers described above, we planned to next synthesize a series of copolymers comprising EtOx and *i*PrOx in order to explore the hydrophilic contribution of EtOx on the LCST of P*i*PrOx (Scheme 1). The respective mixtures of 2-ethyl-2-oxazoline (EtOx$_{25\%}$: 2.19 g, 22.1 mmol; EtOx$_{50\%}$: 4.38 g, 44.2 mmol; EtOx$_{75\%}$: 6.57 g, 66.3 mmol) and 2-isopropyl-2-oxazoline (*i*PrOx$_{75\%}$: 7.5 g, 66.3 mmol; *i*PrOx$_{50\%}$: 5 g, 44.2 mmol; *i*PrOx$_{25\%}$: 2.5 g, 22.1 mmol) were added to a solution of MeOTs (0.186 g, 1.0 mmol) in acetonitrile (30 mL) and polymerized at 42 °C, as in the case of the two homopolymers (PEtOx and P*i*PrOx). The synthesis results of three copolymers (P(EtOx$_{25\%}$*i*PrOx$_{75\%}$), P(EtOx$_{50\%}$*i*PrOx$_{50\%}$), and P(EtOx$_{75\%}$*i*PrOx$_{25\%}$)) including two homopolymers with the same initial monomer/initiator ratio (DP$_{calc}$ = 88.4) are summarized in Table 1. The polymerization behaviors of the copolymers with the initial EtOx and *i*PrOx molar ratios of 25%:75%, 50%:50%, and 75%:25% were characterized by the time-dependent change in the DP and PDI via the MALDI-TOF mass and GPC traces, as seen in Figure 4. Regardless of the comonomer ratio in the feed, the experimental degree of polymerization (DP from MALDI-TOF mass spectrometry) of the respective copolymers was close to the predicted value from the initial monomer/initiator ratio (DP$_{calc}$ = 88.4) and their

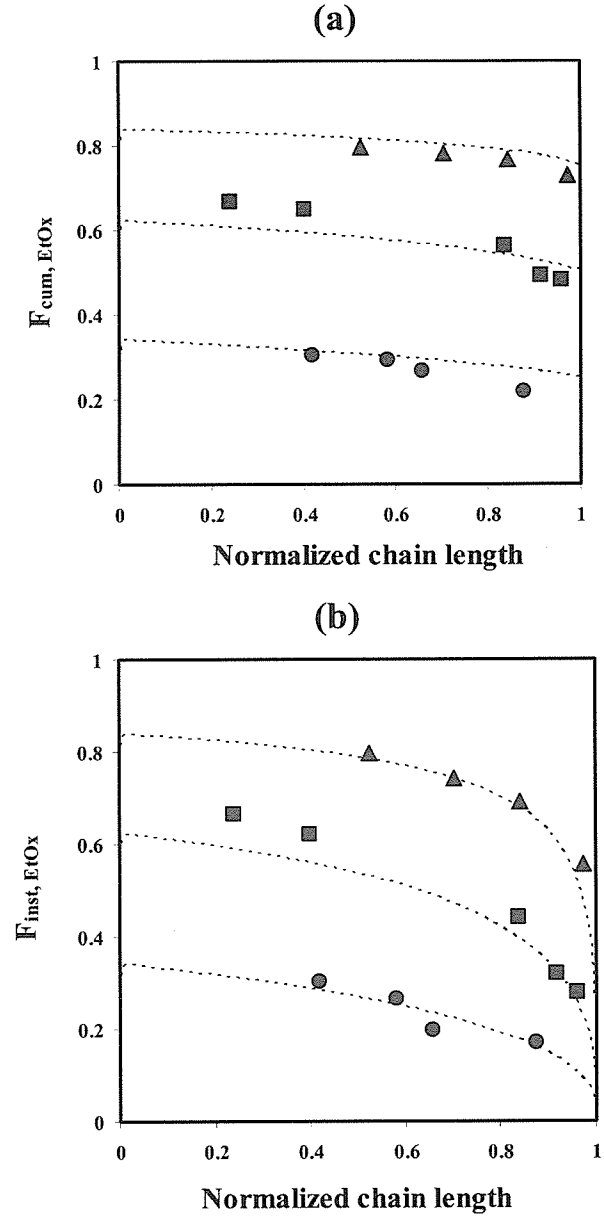

Figure 7. (a) Cumulative ($F_{cum,EtOx}$) and (b) instantaneous ($F_{inst,EtOx}$) composition plots for spontaneous gradient copolymers. The theoretical prediction curves (dotted) were calculated using the simulation program PROCOP[20] (P(EtOx$_{25\%}$*i*PrOx$_{75\%}$) (●), P(EtOx$_{50\%}$*i*PrOx$_{50\%}$) (■), and P(EtOx$_{75\%}$*i*PrOx$_{25\%}$) (▲)).

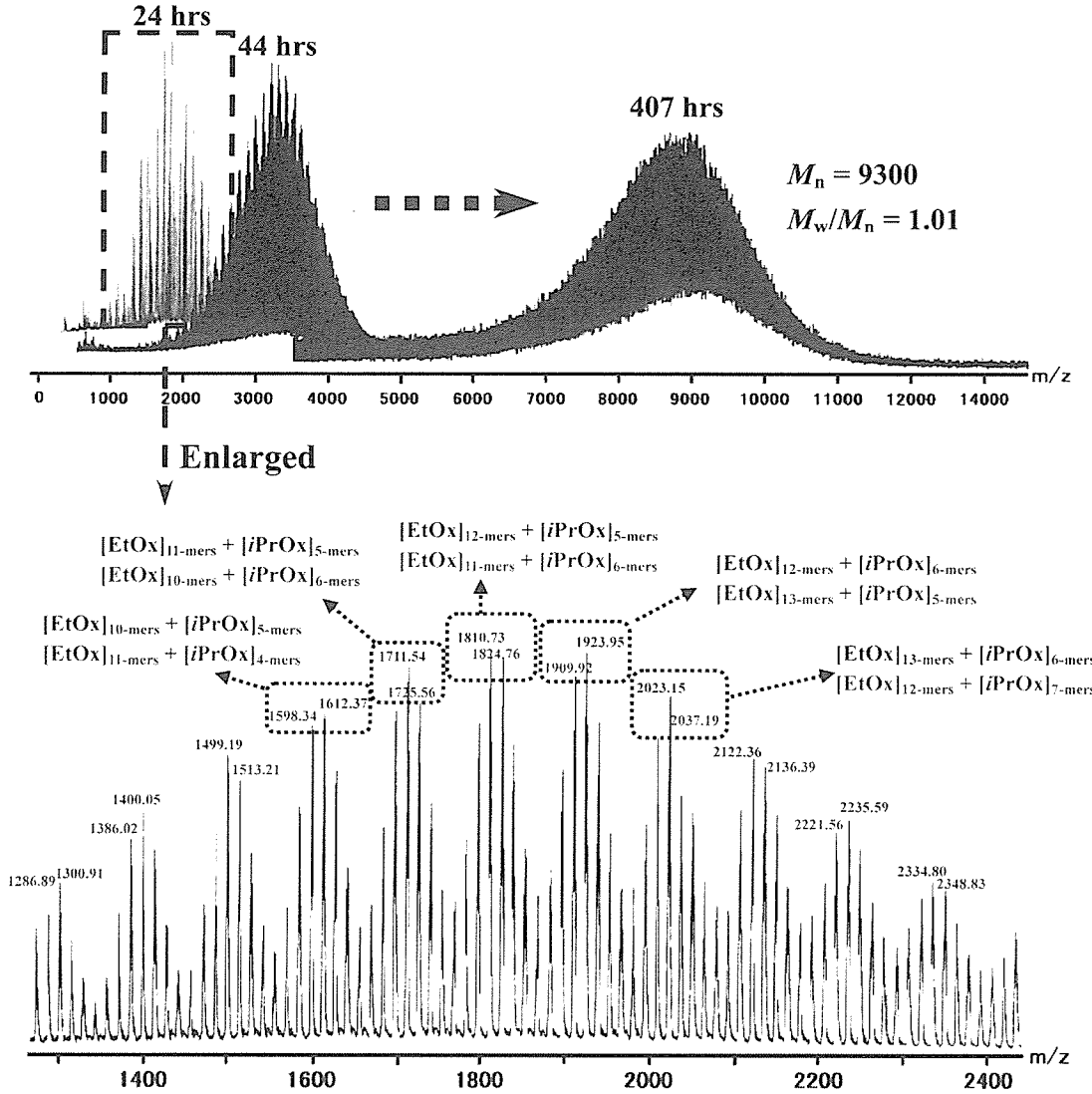

Figure 8. MALDI-TOF mass spectra of gradient copolymer samples comprising $EtOx_{50\%}$ and $iPrOx_{50\%}$ after 24, 44, and 407 h, respectively (upper), and enlarged detail in the mass region of 1300−2400 for the first sampling P($EtOx_{50\%}$-*i*-$PrOx_{50\%}$) after 24 h (lower).

molecular weight distributions were appreciably narrow in all cases (Figure 4). The GPC traces of the three copolymers with different monomer ratios in the feed (P($EtOx_{25\%}$-*i*-$PrOx_{75\%}$), P($EtOx_{50\%}$-*i*-$PrOx_{50\%}$), and P($EtOx_{75\%}$-*i*-$PrOx_{25\%}$)), which were sampled at different polymerization times, also showed an increase in the molar mass with time and symmetrical monomodal peaks, as shown in Figure 5a−c. In addition, the compositions of the final copolymer products determined by ^{1}H NMR spectrometry were in good agreement with the calculated values from the feed ratio of both monomers, indicating their quantitative conversion into the respective copolymers (Figure 6 and Table 1).

In this living polymerization system, copolymers are expected to have a gradient composition, providing sufficiently different reactivity ratios of the two monomers, EtOx and *i*PrOx. Indeed, from the composition analysis by ^{1}H NMR spectrometry of the respective copolymer samplings (monomer conversions: ca. 20%−40%) plotted in Figure 4, the reactivity ratios of the respective monomers were calculated to be r_{EtOx} = 1.78 and r_{iPrOx} = 0.79 through the nonlinear Tidwell−Mortimer (TM) method, showing the most reasonable result among the well-established calculation methods for the further composition analysis of the copolymers (For the details on the determination of the reactivity ratios, see Tables S1 and S2 in the Supporting Information.) While in a conventional process the monomer reactivity ratios can be measured at low conversion (≤ca. 10%) with different monomer feeds, in the living process high polymer is not formed immediately in the reaction. Besides, measurements at such a low conversion could be also affected by the different reactivity of the initiator against a specific monomer. For this reason, the reactivity ratios should be calculated at comparatively higher monomer conversions (20% or higher).[13,18] As far as the polymerization of 2-oxazolines is concerned, it is also well-known that the initial polymerization rate can be different from the terminal polymerization rate,[19] so that we selected monomer conversions of ca. 20%−40% as a reasonable interval in this living system. This difference in the reactivity ratios of two monomers indicates that EtOx should initially be consumed much faster than *i*PrOx. However, because of the decreasing concentration of the former in the residual feed, the rate of its incorporation into the polymer chain also decreased. This resulted in an increased instantaneous incorporation of *i*PrOx into the copolymer as the reaction progressed and ultimately in the formation of an *i*PrOx-rich chain end. Because of the simultaneous initiation and uniform propagation kinetics in this living system as known from the appreciably low polydispersity indices ($M_w/M_n \leq 1.02$), each polymer chain should display a similar trend of a gradually decreasing EtOx and an increasing *i*PrOx composition along the backbone from the α-terminal to active ω-chain end. The cumulative and

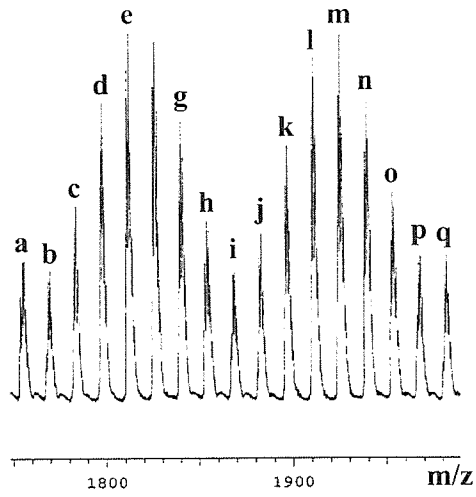

Assign.	$Mass_{calc.}$	$Mass_{exp.}$
a. $[EtOx]_{16\text{-mers}} + [iPrOx]_{1\text{-mers}}$	1754.270	1754.62
b. $[EtOx]_{15\text{-mers}} + [iPrOx]_{2\text{-mers}}$	1768.298	1768.65
c. $[EtOx]_{14\text{-mers}} + [iPrOx]_{3\text{-mers}}$	1782.326	1782.65
d. $[EtOx]_{13\text{-mers}} + [iPrOx]_{4\text{-mers}}$	1796.354	1796.69
e. $[EtOx]_{12\text{-mers}} + [iPrOx]_{5\text{-mers}}$	1810.382	1810.73
f. $[EtOx]_{11\text{-mers}} + [iPrOx]_{6\text{-mers}}$	1824.410	1824.76
g. $[EtOx]_{10\text{-mers}} + [iPrOx]_{7\text{-mers}}$	1838.438	1838.79
h. $[EtOx]_{9\text{-mers}} + [iPrOx]_{8\text{-mers}}$	1852.466	1852.83
i. $[EtOx]_{16\text{-mers}} + [iPrOx]_{2\text{-mers}}$	1867.428	1867.84
j. $[EtOx]_{15\text{-mers}} + [iPrOx]_{3\text{-mers}}$	1881.456	1881.87
k. $[EtOx]_{14\text{-mers}} + [iPrOx]_{4\text{-mers}}$	1895.484	1895.88
l. $[EtOx]_{13\text{-mers}} + [iPrOx]_{5\text{-mers}}$	1909.512	1909.92
m. $[EtOx]_{12\text{-mers}} + [iPrOx]_{6\text{-mers}}$	1923.540	1923.95
n. $[EtOx]_{11\text{-mers}} + [iPrOx]_{7\text{-mers}}$	1937.568	1937.99
o. $[EtOx]_{10\text{-mers}} + [iPrOx]_{8\text{-mers}}$	1951.596	1952.02
p. $[EtOx]_{9\text{-mers}} + [iPrOx]_{9\text{-mers}}$	1965.624	1966.05
q. $[EtOx]_{16\text{-mers}} + [iPrOx]_{3\text{-mers}}$	1980.586	1981.07

Figure 9. Enlarged detail of MALDI-TOF mass spectrum in the region of 1750−1990 (m/z) for gradient copolymer sample comprising $EtOx_{50\%}$ and $iPrOx_{50\%}$ after 24 h (left) and assignment of mass spectral peaks (right).

instantaneous composition plots ($F_{cum,EtOx}$ and $F_{inst,EtOx}$, respectively) vs the normalized chain length were obtained for the three copolymerizations with different initial molar ratios of EtOx and *i*PrOx in the feed (Figure 7). According to the plots, the shape of the obtained gradient copolymers closely followed the theoretical predictions using $r_{EtOx} = 1.78$ and $r_{iPrOx} = 0.79$.[20] In particular, the plots of the instantaneous composition vs normalized chain length showed the dependence of the gradient shapes on the initial feed composition. When the initial feed ratio of EtOx and *i*PrOx was varied from 75%:25% to 25%:75%, no significant continuous change in the instantaneous composition was observed, suggesting the gentle slope of the gradient along the copolymer main chain. The feasibility of this type of methodology has been well-known to trace the composition drift of gradient copolymers in the example of atom transfer radical polymerization (ATRP) living system.[13]

In addition, a series of MALDI-TOF mass spectra for $P(EtOx_{50\%}iPrOx_{50\%})$, which were sampled at different polymerization times, were obtained as shown in Figure 8, showing a good coincidence with the results of the GPC traces. When viewing the copolymers by mass spectra, the relative abundance of all the copolymers with a defined chain length reflects the information about the sequence and composition present in the copolymer.[21] The MALDI-TOF mass spectrometry thus provided a useful method to evaluate these two quantities with good precision, comparing the theoretical mass values and relative intensities for a specific copolymer with the experimental mass spectrum. The series of all the copolymer samplings with the chain lengths below ca. $M_n = 10\,000$ could provide comparatively clearer mass spectra, and the enlarged mass spectrum of $P(EtOx_{50\%}iPrOx_{50\%})$ sampled after 24 h was selected for the detailed analysis of copolymer composition and sequence distribution (Figure 8). All the peaks shown in the mass spectrum of Figure 8 were assigned to copolymers comprised of the EtOx and *i*PrOx monomer units with both methyl groups at the α-terminals and hydroxyl groups at the ω-terminals. The calculated mass of each copolymer is expressed by the following equation:

$$\begin{aligned} mass_{calc} &= [EtOx]_{m-mers} + [iPrOx]_{n-mers} \\ &= \Delta[EtOx]_m + \Delta[iPrOx]_n + \\ &[\alpha\text{-methyl and } \omega\text{-hydroxyl groups}] + [Na^+] \end{aligned}$$

where $mass_{calc}$ (m/z) is the calculated mass of a copolymer with degree of polymerization nearest the measured value, Δ[EtOx] (or Δ[*i*PrOx]) is the mass of the monomer unit, and $[Na^+]$ is the mass of a sodium ion. The detailed peak assignments are summarized in Table 2, where $mass_{exp}$ is the experimental mass value of the most and second intense signals among the respective homologue series in the mass region of 1300−2400. For instance, the strongest signal ($mass_{exp} = 1810.73$) and second most intense signal ($mass_{exp} = 1824.76$) in the mass region of 1750−1990 were in good agreement with the calculated mass values of the two corresponding copolymers, as shown below.

$$[EtOx]_{12-mers} + [iPrOx]_{5-mers} = 99.13 \times 12 + 113.158 \times 5 + 32.042 + 22.99 = 1810.382$$

$$[EtOx]_{11-mers} + [iPrOx]_{6-mers} = 99.13 \times 11 + 113.158 \times 6 + 32.042 + 22.99 = 1824.410$$

A more detailed assignment for all the mass spectral peaks in the region of 1750−1990 is also presented in Figure 9. Similar results for the other two gradient copolymers ($P(EtOx_{25\%}iPrOx_{75\%})$ and $P(EtOx_{75\%}iPrOx_{25\%})$) with different monomer ratios in the feed were also confirmed by MALDI-TOF mass spectrometry (Figures S4a−d and S5a−d in the Supporting Information).

In the case that the MALDI-TOF mass spectra were clearly recognized, the contour map exhibiting the number of *i*PrOx units per chain on the abscissa and the number of EtOx units per chain on the ordinate could be obtained by 2D plots using

Table 2. Assignment of MALDI-TOF Mass Spectral Peaks Shown in Figure 8

assignt	$mass_{calc}$	$mass_{exp}$	assignt	$mass_{calc}$	$mass_{exp}$
$[EtOx]_{8-mers} + [iPrOx]_{4-mers}$	1300.704	1300.91	$[EtOx]_{9-mers} + [iPrOx]_{3-mers}$	1286.676	1286.89
$[EtOx]_{9-mers} + [iPrOx]_{4-mers}$	1399.834	1400.05	$[EtOx]_{10-mers} + [iPrOx]_{3-mers}$	1385.806	1386.02
$[EtOx]_{10-mers} + [iPrOx]_{4-mers}$	1498.964	1499.19	$[EtOx]_{9-mers} + [iPrOx]_{5-mers}$	1512.992	1513.21
$[EtOx]_{10-mers} + [iPrOx]_{5-mers}$	1612.122	1612.37	$[EtOx]_{11-mers} + [iPrOx]_{4-mers}$	1598.094	1598.34
$[EtOx]_{11-mers} + [iPrOx]_{5-mers}$	1711.252	1711.54	$[EtOx]_{10-mers} + [iPrOx]_{6-mers}$	1725.280	1725.56
$[EtOx]_{12-mers} + [iPrOx]_{5-mers}$	1810.382	1810.73	$[EtOx]_{11-mers} + [iPrOx]_{6-mers}$	1824.410	1824.76
$[EtOx]_{12-mers} + [iPrOx]_{6-mers}$	1923.540	1923.95	$[EtOx]_{13-mers} + [iPrOx]_{5-mers}$	1909.512	1909.92
$[EtOx]_{13-mers} + [iPrOx]_{6-mers}$	2022.670	2023.15	$[EtOx]_{12-mers} + [iPrOx]_{7-mers}$	2036.698	2037.19
$[EtOx]_{14-mers} + [iPrOx]_{6-mers}$	2121.800	2122.36	$[EtOx]_{13-mers} + [iPrOx]_{7-mers}$	2135.828	2136.39
$[EtOx]_{14-mers} + [iPrOx]_{7-mers}$	2234.958	2235.59	$[EtOx]_{15-mers} + [iPrOx]_{9-mers}$	2220.930	2221.56
$[EtOx]_{15-mers} + [iPrOx]_{7-mers}$	2334.088	2334.80	$[EtOx]_{14-mers} + [iPrOx]_{8-mers}$	2348.116	2348.83

Microsoft Excel 2002 software.[22] After completing the precise mass assignment of all the peaks in the region of 1300−2400 (*m/z*) for the $P(EtOx_{50\%}iPrOx_{50\%})$ sampling after 24 h, the contribution of each monomer unit to the calculated mass value of a copolymer with the degree of polymerization to nearest the measured value was determined, and the relative abundance (or intensity) of the assigned copolymer was represented as a function of the number of EtOx and *i*PrOx units (Figure 10a). From this 2D graph, it was obvious that the amount of EtOx in the copolymer backbone was ca. twice that of *i*PrOx during the initial period of copolymerization (24 h), which was caused by the sufficiently different reactivity ratios of the two monomers. Furthermore, the six contour maps after 24, 44, 70, 168, 265, and 407 h are also represented on the single $x-y$ coordinate system with the similar treatments (Figure 10b). Since it was hard to consider all the mass regions of the copolymer, the specific intervals within the seven lines and seven columns centering on the most intense signals should be selectively exhibited for clarification. The traces of all the contour maps were in good agreement with the result of the composition analysis of the two monomer units by ^1H NMR spectrometry as shown in Figure S6 of the Supporting Information.

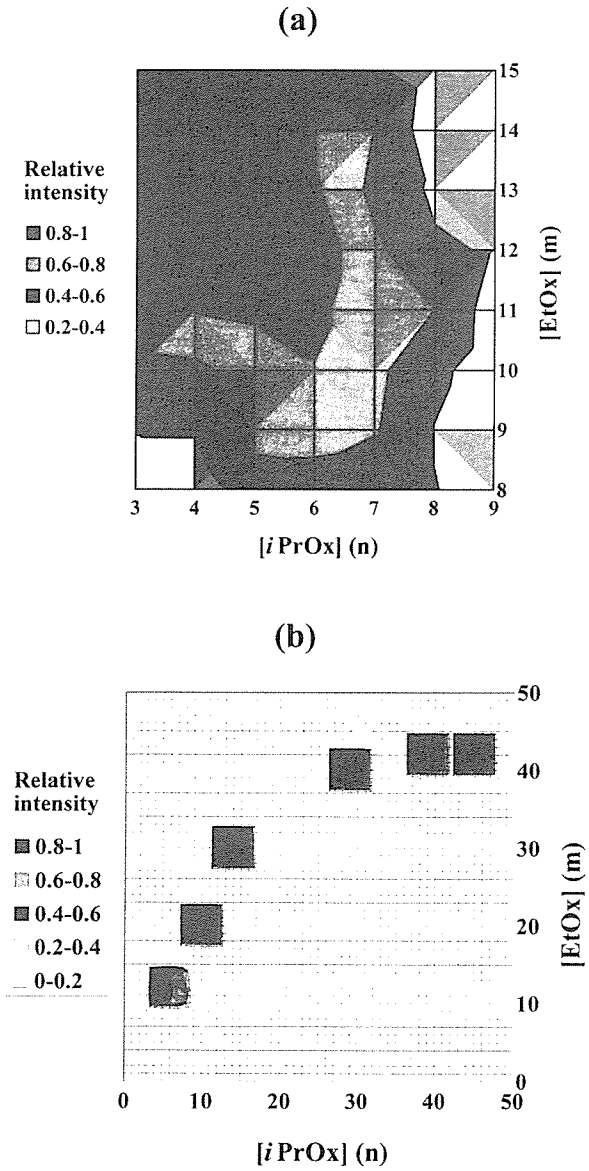

Figure 10. Gradient copolymer fingerprint obtained from MALDI-TOF mass analysis: a contour map showing the number of *i*PrOx units on the abscissa and the number of EtOx units on the ordinate (a) in the mass region of 1300−2400 for the first sampling $P(EtOx_{50\%}iPrOx_{50\%})$ after 24 h and (b) trace of six contour maps obtained after 24, 44, 70, 168, 265, and 407 h.

Determination of the Cloud Points (T_{cp}). The measurement of the changing points in turbidity, defined here as the cloud points (T_{cp}), was adapted to determine the lower critical solution temperature (LCST) of a polymer solution. Figure 11a shows the dependence of the turbidity on the increasing temperature for the (co)polymer solutions with a different EtOx composition. The transmittance sharply decreased at a specific temperature in phosphate-buffered solution (10 mM PBS (pH = 7.4)) in

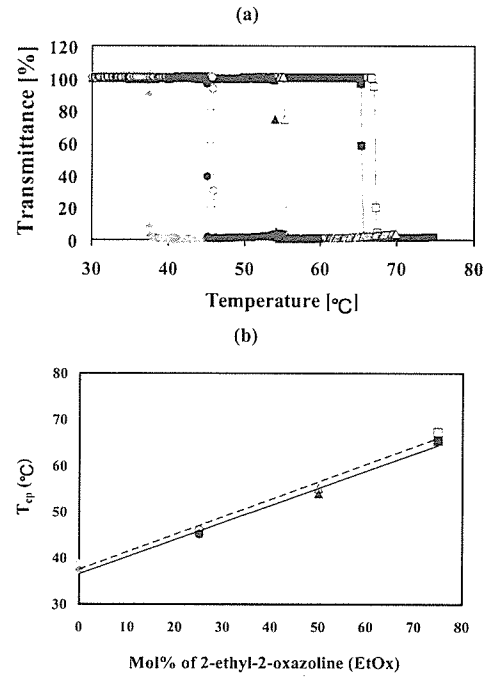

Figure 11. (a) Transmittance changes at 500 nm of 1.0 wt % (co)-polymer solutions ($PiPrOx$ (◆, ◇), $P(EtOx_{25\%}iPrOx_{75\%})$ (●, ○), $P(EtOx_{50\%}iPrOx_{50\%})$ (▲, △), and $P(EtOx_{75\%}iPrOx_{25\%})$ (■, □)) as a function of temperature (10 mM PBS (pH = 7.4) in the absence (open shape) or presence (closed shape) of 150 mM NaCl, rate 0.5 °C/min). (b) Relationship between cloud point (T_{cp}) and comonomer (EtOx) composition in the (co)polymers.

the absence (open symbols) or presence (closed symbols) of 150 mM NaCl, indicating a sharp LCST-type phase transition. The LCST values were found to linearly increase with the increasing mol % of EtOx (n), from 38.7 °C (or 37.4 °C) at n = 0% to 67.3 °C (or 65.4 °C) at n = 75% for a 1.0 wt % polymer solution in the absence (or presence) of 150 mM NaCl (Figure 11b). Regardless of the *i*PrOx to EtOx ratio, an exceedingly clear sensitivity of the phase separation was observed in all cases, whereas no change in transmittance appeared in the case of a PEtOx homopolymer at the measured temperatures up to 90 °C (Table 1). It was also observed that the LCST values of the (co)polymer solutions in the presence of 150 mM NaCl, viz., near the physiological condition, slightly shifted to lower temperatures in all cases compared to that in the absence of NaCl. This result was in agreement with the well-known "salting-out" effect of NaCl.[23]

A notable point of these turbidity results is that observed transition was appreciably sharp and simply correlated with the ratio of both monomers in the copolymers even though they have the compositional gradient along the polymer strand. It may be reasonable to assume that the LCST property of such a gradient copolymer may become complicated due to a possible formation of micelle-like molecular association derived from a deviating amphiphilicity along the polymer chain. Nevertheless, the static light scattering (SLS) measurements of the solution with varying temperature provided no obvious sign of assembly formation, keeping the weak and constant scattering intensity up to the LCST (data not shown). Although we may not exclude the possibility of conformational change in a single strand of the gradient copolymers below LCST due to the deviating amphiphilicity in the strand, turbidity behavior follows a rather simple and practical rule to be correlated with the ratio of both monomers in the copolymers. Detailed solution behavior of these gradient copolymers should be an important topic for the further study to understand their actual molecular dynamics related to temperature change, yet the present study recalls the well-established oxazoline polymerization as a convenient procedure to obtain the copolymers with extremely narrow molecular weight distribution and finely tuned LCST.

Conclusions

This study developed the facile and precise synthetic route of thermosensitive POx gradient copolymers via the living cationic polymerization of 2-isopropyl-2-oxazoline (*i*PrOx) mixed with a specific composition of 2-ethyl-2-oxazoline (EtOx) as a hydrophilic comonomer. The oxazoline monomers (EtOx and *i*PrOx) had sufficiently different reactivity ratios of 1.78 and 0.79, respectively, leading to obtain the gradient copolymers with varying composition and very narrow molecular weight distribution. Turbidity measurements revealed that LCST of the gradient copolymers can be minutely modulated over a broad range of temperature from 38.7 to 67.3 °C simply by varying the molar ratio of EtOx to *i*PrOx. This approach of copolymerizing a variety of oxazoline monomers with different hydrophobic and hydrophilic balance, in a condition to attain living polymerization (mild temperature in acetonitrile), apparently lead to the systematic preparation of versatile end-functionalized polyoxazoline derivatives with finely tuned LCST, which have a promising feasibility particularly in biomedical applications as constructing thermosensitive bioconjugates and drug delivery systems.

Acknowledgment. This work was financially supported by Special Coordination Funds for Science and Technology from the Ministry of Education, Culture, Sports, Science and Technology of Japan (MEXT) as well as by the Core Research for Evolutional Science and Technology (CREST) from the Japan Science and Technology Agency (JST).

Supporting Information Available: Figures S1−S6 and Tables S1 and S2. This material is available free of charge via the Internet at http://pubs.acs.org.

References and Notes

(1) (a) Bergbreiter, D. E.; Osburn, P. L.; Wilson, A.; Sink, E. M. *J. Am. Chem. Soc.* **2000**, *122*, 9058. (b) Hamamoto, H.; Suzuki, Y.; Yamada, Y.; Tabata, H.; Takahashi, H.; Ikegami, S. *Angew. Chem., Int. Ed.* **2005**, *44*, 4536.

(2) (a) Uchiyama, S.; Kawai, N.; de Silva, A. P.; Iwai, K. *J. Am. Chem. Soc.* **2004**, *126*, 3032. (b) Hu, Z. B.; Chen, Y. Y.; Wang, C. J.; Zheng, Y. D.; Li, Y. *Nature (London)* **1998**, *393*, 149.

(3) (a) Kanazawa, H.; Yamamoto, K.; Matsushima, Y.; Takai, N.; Kikuchi, A.; Sakurai, Y.; Okano, T. *Anal. Chem.* **1996**, *68*, 100. (b) Kikuchi, A.; Okano, T. *Prog. Polym. Sci.* **2002**, *27*, 1165.

(4) (a) Stayton, P. S.; Shimoboji, T.; Long, C.; Chilkoti, A.; Chen, G.; Harris, J. M.; Hoffman, A. S. *Nature (London)* **1995**, *378*, 472. (b) Matsukata, M.; Aoki, T.; Sanui, K.; Ogata, N.; Kikuchi, A.; Sakurai, Y.; Okano, T. *Bioconjugate Chem.* **1996**, *7*, 96. (c) Ding, Z.; Chen, G.; Hoffman, A. S. *J. Biomed. Mater. Res.* **1998**, *39*, 498.

(5) (a) Yoshida, R.; Sakai, T.; Okano, T.; Sakurai, Y.; Bae, Y. H.; Kim, S. W. *J. Biomater. Sci., Polym. Ed.* **1991**, *3*, 155. (b) Cammas, S.; Suzuki, K.; Sone, Y.; Kakurai, Y.; Kataoka, K.; Okano, T. *J. Controlled Release* **1997**, *48*, 157. (c) Kono, K. *Adv. Drug. Deliv. Rev.* **2001**, *53*, 307.

(6) (a) Park, J. S.; Akiyama, Y.; Winnik, F. M.; Kataoka, K. *Macromolecules* **2004**, *37*, 6786. (b) Diab, C.; Akiyama, Y.; Kataoka, K.; Winnik, F. M. *Macromolecules* **2004**, *37*, 2556.

(7) (a) Kobayashi, S. *Prog. Polym. Sci.* **1990**, *15*, 751. (b) Aoi, K.; Okada, M. *Prog. Polym. Sci.* **1996**, *21*, 151. (c) Kobayashi, S.; Uyama, H. *J. Polym. Sci., Part A: Polym. Chem.* **2002**, *40*, 192.

(8) (a) Heskins, M.; Guillent, J. E.; James, E. J. *J. Macromol. Sci., Chem.* **1968**, *A2*, 1441. (b) Schild, H. G. *Prog. Polym. Sci.* **1992**, *17*, 163.

(9) (a) Woodle, M. C.; Engbers, C. M.; Zalipsky, S. *Bioconjugate Chem.* **1994**, *5*, 493. (b) Zalipsky, S.; Hansen, C. B.; Oaks, J. M.; Allen, T. M. *J. Pharm. Sci.* **1996**, *85*, 133.

(10) (a) Taylor, L. D.; Cerankowski, L. D. *J. Polym. Sci.* **1975**, *13*, 2551. (b) Feil, H.; Bae, Y. H.; Feijen, J.; Kim, S. W. *Macromolecules* **1993**, *26*, 2496.

(11) (a) Sugihara, S.; Kanaoka, S.; Aoshima, S. *Macromolecules* **2004**, *37*, 1711. (b) Ali, M. M.; Stöver, H. D. H. *Macromolecules* **2004**, *37*, 5219. (c) Mori, H.; Iwaya, H.; Nagai, A.; Endo, T. *Chem. Commun.* **2005**, *38*, 4872. (d) Lutz, J.; Hoth, A. *Macromolecules* **2006**, *39*, 893.

(12) (a) Kagiya, T.; Matsuda, T.; Nakato, M.; Hirata, R. *J. Macromol. Sci., Chem.* **1972**, *6*, 1631. (b) Cai, G.; Litt, M. *J. Polym. Sci., Part A: Polym. Chem.* **1992**, *30*, 649. (c) Hoogenboom, R.; Fijten, M. W. M.; Schubert, U. S. *J. Polym. Sci., Part A: Polym. Chem.* **2004**, *42*, 1830.

(13) (a) Pakula, T.; Matyjaszewski, K. *Macromol. Theory Simul.* **1996**, *5*, 987. (b) Matyjaszewski, K.; Ziegler, M. J.; Arehart, S. V.; Greszta, D.; Pakula, T. *J. Phys. Org. Chem.* **2000**, *13*, 775.

(14) Seeliger, W.; Aufderhaar, E.; Diepers, W.; Feinauer, R.; Nehring, R.; Their, W.; Hellmann, H. *Angew. Chem., Int. Ed. Engl.* **1966**, *5*, 875.

(15) Perrin, D. D.; Armarego, W. L. F.; Perrin, D. R. *Purification of Laboratory Chemicals*; Pergamon: Oxford, 1980.

(16) (a) Levy, A.; Litt, M. *J. Polym. Sci., Part A-1* **1968**, *6*, 1883. (b) Litt, M.; Levy, A.; Herz, J. *J. Macromol. Sci., Chem.* **1975**, *A9*, 703. (c) Warakomski, J. M.; Thill, B. P. *J. Polym. Sci., Part A* **1990**, *28*, 3551.

(17) (a) Liu, Q.; Konas, M.; Riffle, J. S. *Macromolecules* **1993**, *26*, 5572. (b) Chen, C. H.; Wilson, J.; Chen, W.; Davis, R. M.; Riffle, J. S. *Polymer* **1994**, *35*, 3587. (c) Kobayashi, S.; Masuda, E.; Shoda, S.; Shimano, Y. *Macromolecules* **1989**, *22*, 2878. (d) Wiesbrock, F.; Hoogenboom, R.; Leenen, M. A. M.; Meier, M. A. R.; Schubert, U. S. *Macromolecules* **2005**, *38*, 5025.

(18) Madruga, E. L. *Prog. Polym. Sci.* **2002**, *27*, 1879.

(19) (a) Saegusa, T.; Ikeda, H.; Fujii, H. *Macromolecules* **1973**, *6*, 315. (b) Saegusa, T.; Kobayashi, S.; Yamada, A. *Makromol. Chem.* **1976**, *177*, 2271. (c) Uyama, H.; Kobayashi, S. *Macromolecules* **1991**, *24*, 614.

(20) Hagipol, C. *Copolymerization-Toward a Systematic Approach*; Kluwer Academic: New York, 1999.

(21) (a) Montaudo, M. S. *Rapid Commun. Mass Spectrom.* **1999**, *13*, 639. (b) Montaudo, M. S. *Mass Spectrom. Rev.* **2002**, *21*, 108.

(22) Terrier, P.; Buchmann, W.; Cheguillaume, G.; Desmazières, B.; Tortajada, J. *Anal. Chem.* **2005**, *77*, 3292.

(23) Lin, P.; Pearce, E. M.; Kwei, T. K. *J. Polym. Sci., Part B: Polym. Phys.* **1988**, *26*, 603.

MA0605548

Journal of Drug Targeting, July 2006; 14(6): 413–424

informa
healthcare

Photochemical enhancement of transgene expression by polymeric micelles incorporating plasmid DNA and dendrimer-based photosensitizer

NOBUHIRO NISHIYAMA[1], ARNIDA[2], WOO-DONG JANG[2], KOTOE DATE[2], KANJIRO MIYATA[2], & KAZUNORI KATAOKA[1,2,3,4]

[1]*Center for Disease Biology and Integrative Medicine, Graduate School of Medicine, The University of Tokyo, 7-3-1 Hongo, Bunkyo-ku, Tokyo 113-0033, Japan,* [2]*Department of Materials Engineering, Graduate School of Engineering, The University of Tokyo, 7-3-1 Hongo, Bunkyo-ku, Tokyo 113-8656, Japan,* [3]*Core Research Program for Evolutional Science and Technology (CREST), Japan Science and Technology Agency (JST), Tokyo, Japan, and* [4]*Center for NanoBio Integration, The University of Tokyo, 7-3-1 Hongo, Bunkyo-ku, Tokyo 113-8656, Japan*

(Received 15 November 2005; revised 19 January 2006; in final form 2 February 2006)

Abstract

The development of synthetic gene carriers has recently received much attention; however, they might lack the ability to control the transgene expression. The use of external stimuli for enhancement of the transgene expression may be a promising approach for the site-directed transfection *in vivo*. In this regard, a new technology of "photochemical internalization (PCI)" has recently been reported, in which the endosomal escape of gene carriers is assisted by photodamage of the endosomal membrane with co-incubating photosensitizers. To apply this technology for systemic gene delivery, the development of appropriate carrier systems for both the plasmid DNA (pDNA) and photosensitizer is of crucial importance. Also, the photocytotoxicity accompanied by the photochemical enhancement of the gene expression may need to be reduced. In this study, the combinational formulation of polymeric micelles incorporating pDNA and a dendrimer-based photosensitizer (DP) (dendrimer phthalocyanine (DPc)) was applied in the PCI-mediated transfection *in vitro* and then, estimating its potential utility for *in vivo* applications. The PCI using the polymeric micelle system achieved a remarkable photochemical enhancement of the transgene expression while maintaining an approximate 80% cell viability over a wide range of the DPc concentrations and light doses. Thus, this system may be promising for *in vivo* PCI-mediated gene delivery.

Keywords: *Gene therapy, non-viral gene carriers, polymeric micelles, photochemical internalization (PCI), dendrimer*

Introduction

Recently, non-viral gene carriers based on cationic lipids and synthetic polymers have received much attention as an attractive alternative to viral vectors in gene therapy (Merdan et al. 2002; Ogris and Wagner 2002; Pack et al. 2005). In addition to several advantages, such as safety, simplicity of use and ease of mass production, the variety of chemical designs of the constituent lipids and polymers is a strong motivation to develop novel gene carriers. In particular, considerable efforts have been devoted to the development of biocompatible gene carriers, which might show longevity during blood circulation and effectively accumulate at the target site (Ogris and Wagner 2002; Pack et al. 2005). In this regard, a promising approach is the use of poly(ethylene glycol) (PEG)–polycation block copolymers, since they spontaneously associate with plasmid DNA (pDNA) to form the nano-scaled polyplex micelles, in which the pDNA/polycation polyplex core is surrounded by a dense and hydrophilic PEG palisade (Katayose and Kataoka 1997; Harada-Shiba et al. 2002; Itaka et al. 2003; Miyata et al. 2004; Wakebayashi et al. 2004; Fukushima et al. 2005). Indeed, the polyplex micelles formed between pDNA and PEG–poly(L-lysine)

Correspondence: K. Kataoka, Department of Materials Engineering, Graduate School of Engineering, The University of Tokyo, 7-3-1 Hongo, Bunkyo-ku, Tokyo 113-8656, Japan. E-mail: kataoka@bmw.t.u-tokyo.ac.jp

ISSN 1061-186X print/ISSN 1029-2330 online © 2006 Informa UK Ltd.
DOI: 10.1080/10611860600834508

(A)

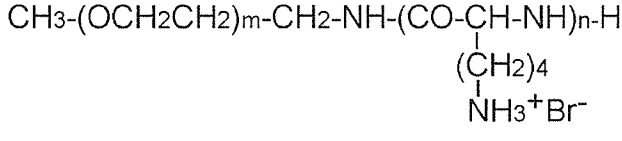

(B)

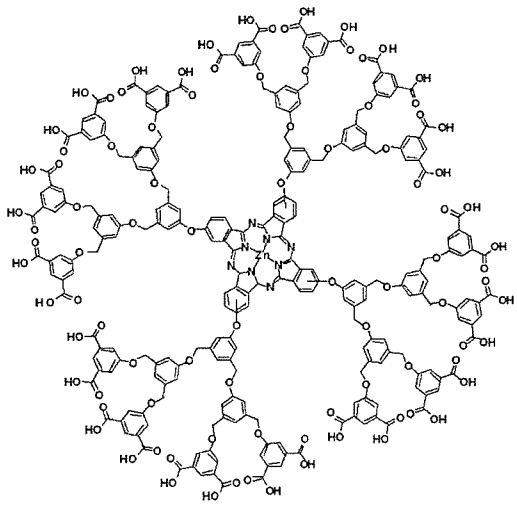

Figure 1. Chemical structures of PEG–PLL block copolymer (A) and DPc (B).

(PEG–PLL) block copolymers (Figure 1(A)) showed an improved stability in proteinous media (Itaka et al. 2003) and prolonged blood circulation in mice (Harada-Shiba et al. 2002). However, the limited transfection ability of the pDNA/PEG–PLL polyplex micelle is a major issue in their applications for *in vivo* gene therapy (Harada-Shiba et al. 2002; Itaka et al. 2003; Miyata et al. 2004). It has been suggested that such a low gene transferring ability of the polyplex micelles might be due to their inefficient transport from the endosome/lysosome to the cytoplasm (Itaka et al. 2003; Miyata et al. 2004).

Other than a high transfection efficiency, site-specific gene transfer has been strongly desired for gene vectors to ensure the safety and effectiveness for *in vivo* gene therapy. However, the existing vectors including viral and non-viral ones still have the problem of non-specific gene transfection. Recently, a smart approach called "photochemical internalization (PCI)" was introduced by Høgset and Berg et al. to overcome both the limited transfection efficiency and the lack of specificity of non-viral gene vectors. The PCI using hydrophilic photosensitizers allows the photochemical disruption of the endosomal/lysosomal membranes, facilitating the cytoplasmic delivery of macromolecular compounds such as genes and proteins (Berg et al. 1999; Høgset et al. 2000, 2002, 2004; Prasmickaite et al. 2001). This approach indeed achieved an appreciable increase in the transfection efficiency upon light illumination under *in vitro* conditions; however, it was accompanied by the problem of photocytotoxicity (Høgset et al. 2000). It should be noted that the photocytotoxicity might not be directly correlated with the photodamage to the endosomal/lysosomal membranes, but the photodamaging of other susceptible organelles may account for the cytotoxicity involved in the PCI (Macdonald and Dougherty 2001; Moan et al. 1994). Hence, the spatially localized photodamage limited to the endosome/lysosome is assumed to lead to the enhanced photochemical transfection with reduced cytotoxicity (Nishiyama et al. 2005). Also, in addition to controlled localization in the intracellular compartment, photosensitizers might need to be systemically delivered to the target tissue to achieve a successful PCI-mediated gene delivery *in vivo*.

In this study, the PCI using polymeric micelles incorporating DPs (dendrimer phthalocyanine (DPc) illustrated in Figure 1(B)) was carried out to enhance the gene transferring ability of the aforementioned pDNA/PEG–PLL polyplex micelle in a light-selective manner (Figure 2). DPc possesses a center phthalocyanine molecule surrounded by a second generation of aryl ether dendrons and 32 carboxyl groups on the periphery of the DPc allow the formation of polyion complex (PIC) micelles through an electrostatic interaction with the PEG–PLL block copolymers

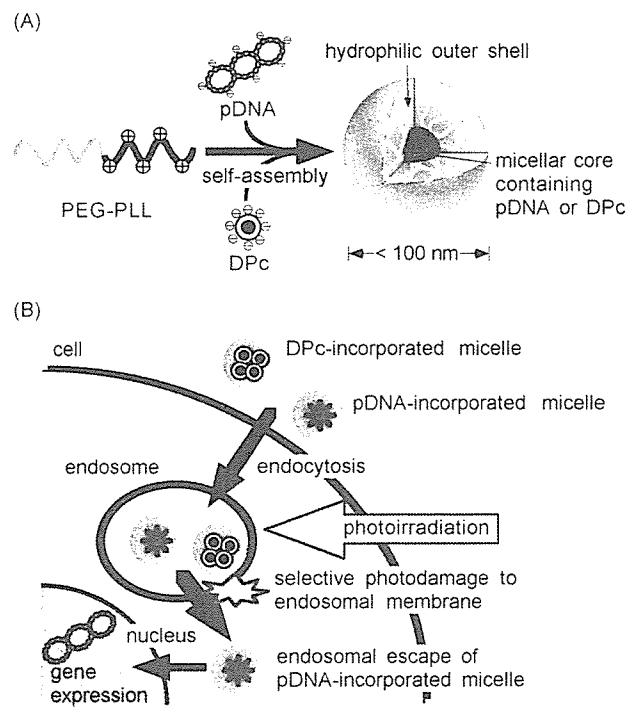

Figure 2. (A) Formation of polymeric micelles through the electrostatic interaction between PEG–PLL and pDNA or DPc. (B) Scheme for itinerary of the pDNA- and DPc-incorporated micelles in the PCI-mediated transfection. Both polymeric micelles are assumed to be taken up by the cell through the endocytic pathway and the localization of the DPc-incorporated micelles in the endosome may allow the selective photodamaging of the endosomal membrane upon photoirradiation, thereby inducing the cytoplasmic delivery of the pDNA-incorporated micelles.

(Stapert et al. 2000; Ideta et al. 2005; Jang et al. 2005). In this strategy, both the pDNA- and DPc-incorporated polymeric micelles are expected to exhibit prolonged blood circulation after intravenous administration and selectively accumulate in the target tissues such as solid tumors as previously reported (Kwon et al. 1994; Nishiyama et al. 2003a,b; Bae et al. 2005). Also, both micelles are assumed to show the same subcellular localization at the target site due to similar particle sizes and surface properties. The control of the localization of the photosensitizers and gene carriers at both the tissue and subcellular levels appears to be a prerequisite for the PCI-mediated gene delivery *in vivo*. Furthermore, the DPc-incorporated micelles may cause highly selective photodamage to the endosomal/lysosomal membranes, because polymeric micelles are assumed to be taken up by the cell through the endocytic pathway (Figure 2(B)). Thus, the combinational use of the pDNA- and DPc-incorporated micelles may be a promising approach to the PCI-mediated gene delivery. In the present study, the feasibility of our strategy was confirmed by the enhanced *in vitro* transfection with limited cytotoxicity under different conditions, thus featuring the possibilities for future *in vivo* applications.

Materials and methods

Materials

N^{ε}-Z-L-Lysine and bis(trichloromethyl) carbonate (triphosgene), for the synthesis of PEG–PLL, were purchased from Sigma-Aldrich Co., Inc. (St Louis, MO) and Tokyo Kasei Co., Ltd (Tokyo, Japan), respectively. α-Methoxy-ω-amino-poly(ethylene glycol) (MeO–PEG–NH_2, MW = 12 kg/mol) was purchased from Nippon Oil and Fats, Co., Ltd. Chemicals for the dendrimer synthesis were purchased from Tokyo Kasei and Sigma-Aldrich. *n*-Pentanol and 1,8-diazabicyclo-(5,4,0)-undec-7-ene (DBU) were purchased from Tokyo Kasei and used without further purification. All solvents for the polymer syntheses were distilled just before use.

A pDNA, pCAcc + Luc, containing a firefly luciferase cDNA driven by a CAG promoter (Niwa et al. 1991) was provided by the RIKEN Bioresource Center (Tsukuba, Japan). pDNA was amplified in competent DH5α *Escherichia coli* and purified by a HiSpeed Plasmid Maxi Kit from Qiagen Co., Inc. (Valencia, CA). Sulfonated aluminum phthalocyanine ($AlPcS_{2a}$) (aluminum phthalocyanine with two sulfonate groups on adjacent phthalate rings) was purchased from Frontier Scientific Co., Inc. (Logan, UT).

Polymer synthesis and characterization

The synthesis of the ionic DPc was performed according to the method reported by Ng's group (Ng et al. 1999). The second generation of dendritic phenol was reacted with 4-nitrophthalonitrile by an alkali-mediated coupling reaction to obtain the corresponding dendritic phthalonitrile, which was then treated with $Zn(OAc)_2$ and DBU in *n*-pentanol to give DPc. The obtained DPc was treated with a THF/H_2O mixture solution containing NaOH to obtain the ionic DPc (MW: 4904). The absorption spectra in an aqueous solution revealed that DPc exhibits a B band absorption at 350 nm and a strong Q band absorption at 685 nm, indicating a monomeric dispersion without agglomerization.

PEG–PLL block copolymers (PEG: MW = 12 kg/mol) having different polymerization degrees of the PLL segment (49 and 73; the code names are 12–49 and 12–73, respectively) were synthesized as previously reported (Harada and Kataoka 1995). Briefly, the *N*-carboxy anhydride of N^{ε}-Z-L-lysine was polymerized from the ω-NH_2 group of CH_3O–PEG–NH_2 in DMF under Ar to obtain PEG–PLL(Z), followed by deprotection of the Z group. The polymerization degree of the PLL segments and the narrowly distributed nature of the synthesized PEG–PLL(Z) were determined by the ^{1}H-NMR and the gel permeation chromatography (GPC), respectively.

Preparation of DPc-incorporated micelles

The DPc-incorporated micelles were prepared by mixing DPc and PEG–PLL 12–49 at a stoichiometric charge ratio. In a typical procedure, PEG–PLL was dissolved in a 10 mM NaH_2PO_4 solution (0.457 ml) and added to DPc in a 10 mM Na_2HPO_4 solution (1.0 ml) to give the solution containing the DPc-incorporated micelles in a 10 mM phosphate buffered solution (pH 7.4). The size and size distribution (polydispersity index) of the micelles were measured by dynamic light scattering (DLS) measurements using a DLS-7000 instrument with a vertically polarized incident beam of 488 nm wavelength from an Ar ion laser (Otsuka Electronics Co., Ltd, Osaka, Japan).

Preparation of pDNA/PEG–PLL polyplex micelles

pDNA and PEG–PLL 12–73 were separately dissolved in a 10 mM Tris–HCl buffer (pH 7.4). The PEG–PLL solution with varying concentrations was then added to the pDNA solution to form the polyplex micelles with different N/P ratios, which denote the ratio of the molar concentration of the cationic amino groups in PEG–PLL to that of the phosphate groups in DNA. The polyplex micelle solution was maintained overnight at ambient temperature before use.

The size and size distribution of the polyplex micelles were measured by the DLS measurement using the DLS-7000. The effect of the N/P ratios on the pDNA condensation in the polyplex micelles was estimated from a decrease in the fluorescence intensity

of ethidium bromide (EtBr) due to the exclusion from the DNA double strand. The polyplex micelle solutions at various N/P ratios were adjusted to 20 μg pDNA/ml with 0.4 μg EtBr/ml by adding 10 mM Tris–HCl buffer containing EtBr. The ratio of the residual molar concentration of EtBr to that of the base pair in pDNA was 0.033. The fluorescence measurements (Ex: 510 nm; Em: 590 nm) were carried out at 25°C using a FP-777 spectrofluorometer from Jasco Co., Ltd (Tokyo, Japan). The results were expressed as the relative fluorescence intensity to the intensity of the free pDNA solution with EtBr.

In vitro *transfection and cytotoxicity assays*

Human cervical carcinoma HeLa cells or human hepatoma HuH-7 cells (10,000 cells) were seeded and cultured on a 24-well culture plate (BD Bioscience, Franklin Lakes, NJ) for 24 h prior to the transfection (cell seeding density: 1400 cells/cm^2). The pDNA/-PEG–PLL polyplex micelle solution prepared at a defined N/P ratio containing 1 μg pDNA and the photosensitizer solutions (i.e. $AlPcS_{2a}$, DPc and DPc-incorporated micelle) with various concentrations were added to the cells in 0.5 ml of Dulbecco's modified Eagle's medium (DMEM) containing 10% fetal bovine serum (FBS), followed by a 6 or 24 h incubation and medium replacement with a fresh one. The culture plates were photoirradiated using a 300 W halogen lamp (fluence rate: 3.0 mW/cm^2) equipped with a band-pass filter (400–700 nm) with increased fluence (2.7–8.1 J/cm^2). After a 48 h post-incubation, the transfection efficiency and cell viability were examined. In the transfection assay, the cells were lysed and the luciferase activity of the lysate was measured using the Luciferase Assay System (Promega, Madison, WI) and a Lumat LB9507 luminometer (Berthold Technologies, Bad Wildbad, Germany). The results are expressed as light units per milligram of cell protein determined by a BCA assay kit (Pierce, Rockford, IL). On the other hand, the cell viability was evaluated by the 3-(4,5-dimethylthiazol-2-yl)-2,5-diphenyltetrazolium bromide (MTT) (Dojindo Laboratories, Kumamoto, Japan) assay.

Results and discussion

In this study, we investigated the feasibility of using polymeric micelles as a nanocarrier for the pDNA and photosensitizer in the PCI-mediated gene delivery *in vitro*. As previously described, a simple mixing of pDNA and PEG–PLL results in the formation of the polyplex micelles (Katayose and Kataoka 1997; Itaka et al. 2003). The size and polydispersity indices of the mixtures prepared at various N/P ratios are shown in Figure 3(A) and (B), indicating the formation of the polyplex micelles with sizes of 90–140 nm and a moderate polydispersity over a broad range of N/P ratios (0.5–6). The histogram analysis in the DLS measurement revealed that the polyplex micelles possess a unimodal size distribution (data not shown). Figure 3(C) shows the effect of the N/P ratios

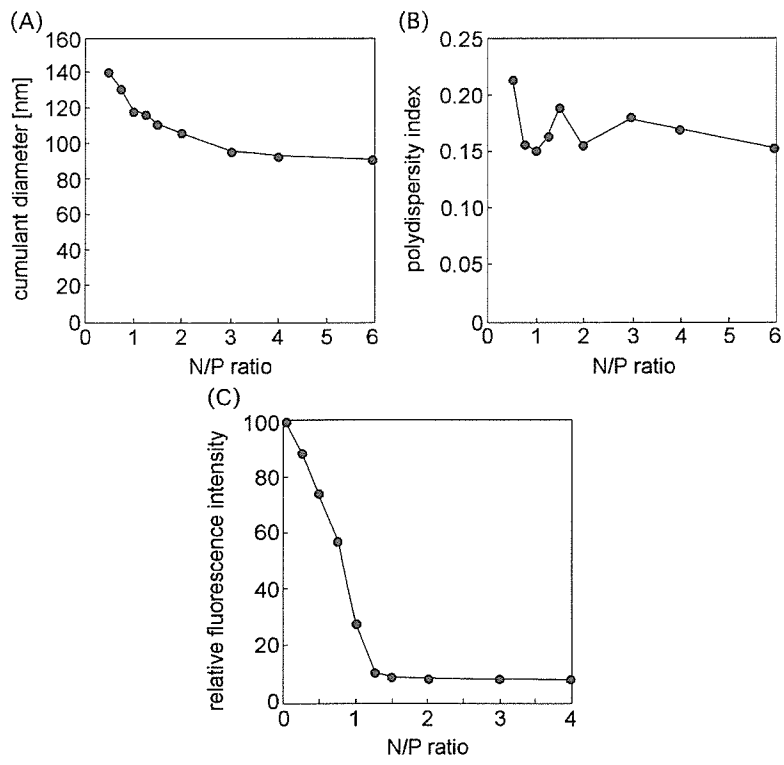

Figure 3. Changes in the cumulant diameter (A), the polydispersity index (μ_2/Γ^2) (B) and the fluorescence intensity of EtBr (C) for the pDNA/PEG–PLL polyplex micelles prepared at different N/P ratios.

on the exclusion of EtBr from the pDNA/PEG–PLL complexes. Apparently, the fluorescence intensity of EtBr leveled off above the N/P ratio of 1.2, suggesting this to be a minimum N/P ratio to fully condense pDNA. On the other hand, it is generally difficult to incorporate conventional photosensitizers into nanocarriers, because they have a hydrophobic structure with a large π-conjugation domain that easily forms aggregates. Recently, we reported DPs as a promising photosensitizer applicable for drug delivery (Nishiyama et al. 2003a,b). DPs have a focal sensitizer core segregated by a 3D dendritic architecture, which might allow effective photochemical reactions even at a high concentration and the periphery with tailored functional groups. Ionic DPs with cationic or anionic peripheral groups show a good solubility in aqueous media and form a PIC micelle with oppositely charged block copolymers (Stapert et al. 2000). We have demonstrated that polymeric micelles incorporating DPs are promising photosensitizer formulations for photodynamic therapy (Ideta et al. 2005; Jang et al. 2005). In the present study, the DPc-incorporated micelles were spontaneously formed through an electrostatic interaction between DPc and PEG–PLL. The DLS measurement revealed that the DPc-incorporated micelles had a diameter of 50 nm with a narrow size distribution (unimodal, polydispersity index (μ_2/Γ^2): 0.12). The DPc-incorporated micelles have strong Q-band absorptions at 630 and 685 nm for excitation of the DPc, thus, expecting a deeper tissue penetration of light for *in vivo* applications.

This study's objective is to investigate the feasibility of the PCI-mediated gene delivery using polymeric micelles as nanocarriers for pDNA and DPc. First, the optimal N/P ratio of the pDNA/PEG–PLL polyplex micelles on the photochemical transfection was determined. Figure 4(A) and (B) show the photochemical enhancement of the transfection of the pDNA/PEG–PLL polyplex micelles prepared at the N/P ratio of 1.2 or 2.0 and the concomitant photocytotoxicity, respectively. In this experiment, HeLa cells were photoirradiated at the fluence of 5.4 J/cm^2 after a 6 h incubation with the combination of the pDNA- and DPc-incorporated micelles and medium replacement with a fresh one, followed by a 48 h post-incubation. The polyplex micelles prepared at N/P = 1.2 achieved more than a 100-fold photochemical enhancement of the gene expression with 20–25% decreases in cell viability, whereas those prepared at N/P = 2.0 showed only a 10–30-fold gene expression enhancement with comparable decreases in cell viability. Thus, the polyplex micelles prepared at N/P = 1.2 might be more efficient in the PCI-mediated transfection compared with those prepared at N/P = 2.0. It should be noted that naked plasmid did not show any detectable gene transfection, regardless of the utilization of the PCI (data not shown), suggesting the necessity of appropriate gene

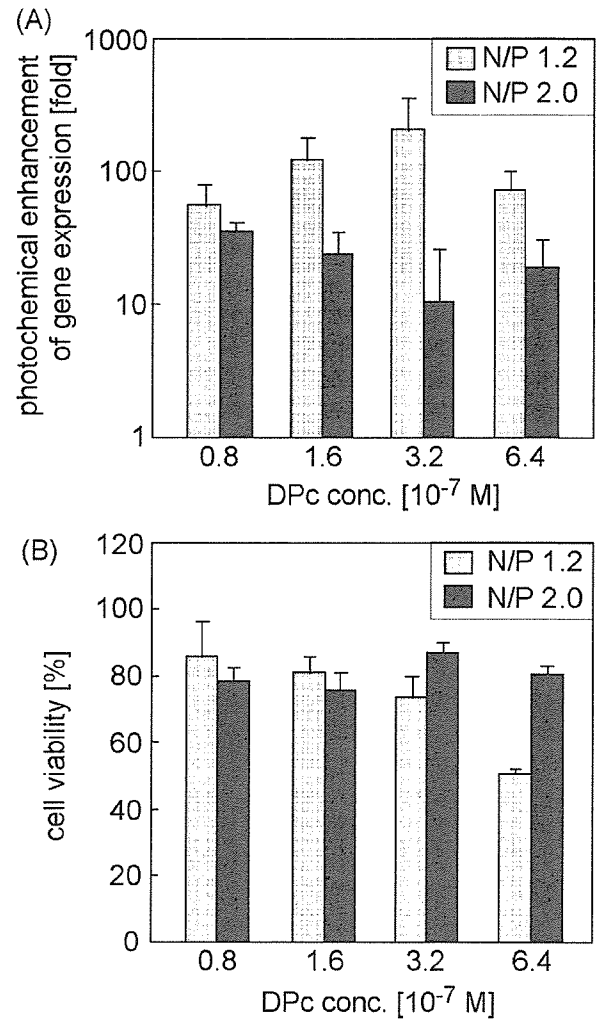

Figure 4. The effect of the N/P ratio of the polyplex micelles on the photochemical enhancement of the gene expression (A) and photocytotoxicity (B) in the PCI-mediated transfection using DPc-incorporated micelle. The light irradiation (fluence: 5.4 J/cm^2) was performed 6 h after incubation with the pDNA- and DPc-incorporated micelles, followed by 48 h post-incubation in a fresh medium.

carriers for the PCI-mediated gene delivery. Interestingly, the polyplex micelles prepared at the N/P ratios of 1.2 and 2.0 showed similar transfection efficiencies in the absence of a photosensitizer and light (5,08,000 ± 1,49,000 vs. 4,17,000 ± 1,69,000 RLU/mg protein (mean ± SD)). These results suggest that an excess of PEG PLL might decrease the efficacy of the photochemical transfection. In the PCI-mediated transfection, the efficient cytoplasmic delivery of the polyplex micelles can be achieved by photochemical rupture of the endosomal membrane; therefore, the release of pDNA from the polyplex micelles in the cytoplasm or nuclei may be a rate-limiting process in the gene transfection. The polyplex micelles at N/P = 1.2 are expected to show more efficient pDNA release than those at N/P = 2.0, thereby showing a higher photochemical enhancement of the transfection. Based on these results,

polyplex micelles prepared at N/P = 1.2 were used for further investigations.

The transfection efficiency and cytotoxicity of the polyplex micelles co-incubated with the DPc-incorporated micelles in the presence or absence of light irradiation (fluence: 5.4 J/cm^2) are shown in Figure 5(A) and (B), respectively. The same experimental procedures as in Figure 4 were applied in this study. Based on these results, the PCI using the DPc-incorporated micelles achieved a 56–212-fold photochemical enhancement of the transfection of the polyplex micelles while maintaining an approximately 80% cell viability over a wide range of DPc concentrations (0.4×10^{-7}–3.2×10^{-7} M) and showed an approximately 50% decrease in viability above the critical DPc concentration (6.4×10^{-7} M). Note that a similar photochemical enhancement of the transfection was observed when 293 T cells were used (data not shown). The maximal transfection level achieved by the PCI using the DPc-incorporated micelles was comparable to that obtained using hydroxychloroquine (hc), which has been demonstrated to be a potent endosomotropic agent (Itaka et al. 2004) (Figure 5(A)). Interestingly, the transfection efficiency of the polyplex micelles decreased as the concentration of the DPc-incorporated micelles increased, particularly under non-irradiated conditions (Figures 5(A) and 6(A)), thus leading to a remarkably high light-selectivity of the gene transfection. Such a DPc concentration-dependent decrease in the transfection efficiency of the polyplex micelles was not observed in the PCI using DPc alone (Figure 7(A)). There may be two possible explanations for this observation. First, the polyplex micelles may compete with the DPc-incorporated micelles in the cellular uptake due to similar particle sizes and surface properties. In Figure 5(A), the molar concentration of the DPc-incorporated micelles was estimated to be comparable to or 20-fold higher than that of the polyplex micelles at the DPc concentration of 2.0×10^{-8} or 6.4×10^{-7} M, respectively. An increase in the DPc concentration decreases the molar ratio of the pDNA-incorporated micelles to the DPc-incorporated micelles in the medium, leading to a decreased cellular uptake of the pDNA-incorporated micelles. Alternatively, the pDNA- and DPc-incorporated micelles may interact each other, thereby decreasing the transfection efficiency. Indeed, we observed in Figure 4(A) that an excess of PEG–PLL could decrease the transfection efficiency of the polyplex micelles in the PCI-mediated transfcetion. These possibilities may also account for the DPc concentration-dependent decrease in the transfection efficiency.

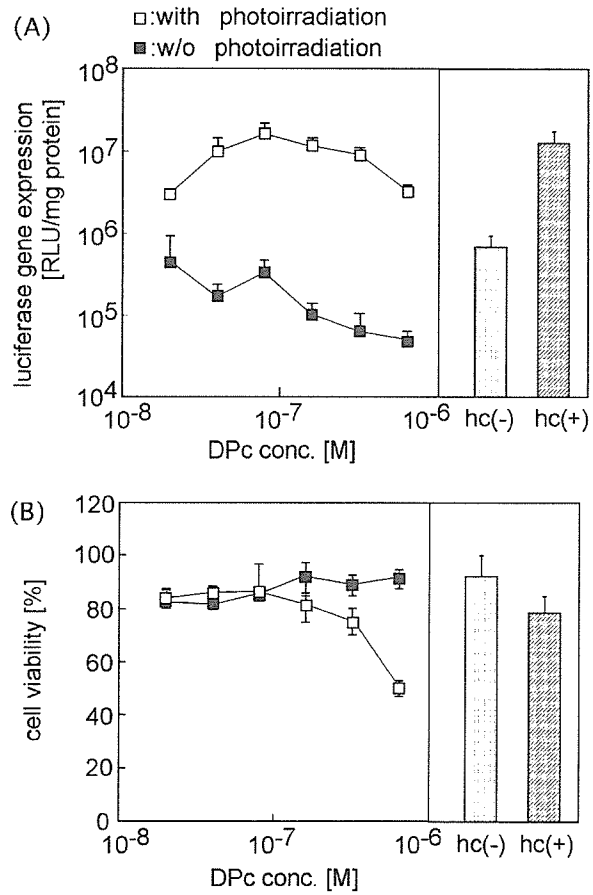

Figure 5. The effect of the DPc concentration on the transfection efficiency (A) and photocytotoxicity (B) in the PCI-mediated transfection using the DPc-incorporated micelles. The light irradiation (fluence: 5.4 J/cm^2) was performed 6 h after incubation with the pDNA- and DPc-incorporated micelles, followed by 48 h post-incubation in a fresh medium.

Regarding changes in cell viability in Figure 5(B), a DPc concentration-dependent decrease in cell viability was observed at the DPc concentrations above 1.6×10^{-7} M, while a DPc concentration-independent 10–20% decrease in cell viability was observed below 1.6×10^{-7} M DPc, regardless of photoirradiation. It is assumed that the DPc concentration-dependent decrease in cell viability observed at the region of high-DPc concentration might be attributable to the photochemical reactions in the PCI-mediated transfection. On the other hand, the 10–20% decrease in cell viability at the lower DPc concentration even without photoirradiation may be inducible by the DPc-incorporated micelles, since the pDNA-incorporated micelles alone did not show an appreciable cytotoxicity (Figures 6(C) and 7(C)). Nevertheless, such a 10–20% decrease in cell viability, of which the mechanisms remain to be clarified yet, is still in a tolerable range and is unlikely to be the serious limitations of this strategy.

The effects of the DPc concentration and fluence on the transfection efficiency of the polyplex micelles, photochemical enhancement of the transfection and photocytotoxicity in the PCI using the DPc-incorporated micelles were completely examined and the results are shown in Figure 6(A)–(C), respectively. Similarly, the PCI-mediated transfection of the pDNA/PEG–PLL polyplex micelles was carried out

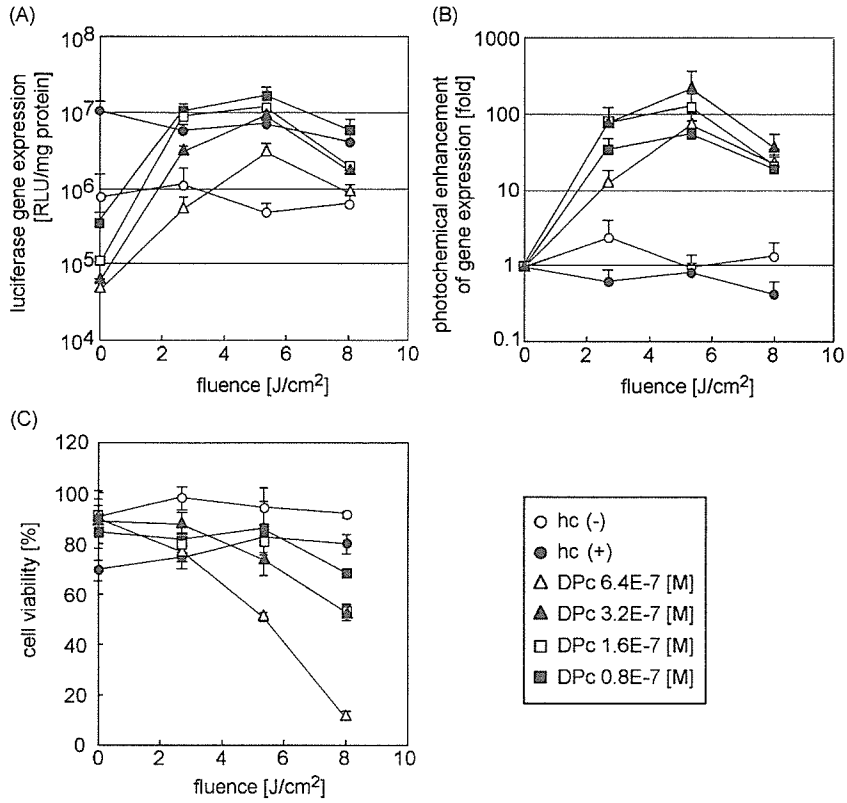

Figure 6. The effects on the DPc concentration and fluence on the transfection efficiency (A), photochemical enhancement of the gene expression (B) and photocytotoxicity (C) in the PCI-mediated transfection using the DPc-incorporated micelles. The light irradiation was performed 6 h after incubation with the pDNA- and DPc-incorporated micelles, followed by 48 h post-incubation in a fresh medium. The "hc" strands for hydroxychloroquine.

using DPc alone or $AlPcS_{2a}$, which was demonstrated to be an effective photosensitizer in the PCI (Høgset et al. 2002, 2004). These results are shown in Figures 7 and 8, respectively. Also, to easily compare the main differences between the results in Figures 6–8, the effects of each photosensitizer on the photochemical enhancement of the gene expression and cell viability at the fluence of 5.4 J/cm^2 are summarized in Table I. In the PCI using DPc alone, the highest transfection efficiency of the polyplex micelles was obtained with a 25–50% reduced cell viability (Figure 7(A) and (C)). The PCI using $AlPcS_{2a}$ showed a transfection activity comparable to that using the DPc-incorporated micelles; however, the photochemical enhancement of the transgene expression was accompanied by an inevitable photocytotoxicity (Figure 8(A) and (C)). Eventually, the PCI using the combination of the pDNA- and DPc-incorporated micelles showed the highest photochemical enhancement of the gene transfection of the polyplex micelles (Figure 6(B)), which may be attributed to the reduced transfection efficiency at comparatively high-concentrations of the DPc-incorporated micelles under non-irradiated conditions as discussed above as well as actual increases in the transfection efficiency. Such a high-light-selectivity of the gene transfection might be advantageous for accomplishing the site-directed gene transfer using the PCI concept. More importantly, the PCI using the DPc-incorporated micelles showed an appreciably wide range of safe DPc concentrations and light doses, in which a remarkable enhancement of the transfection was achieved without a substantial decrease in the cell viability (Figure 6(B) and (C)). The efficacy of this system was prominent even when compared with those of other systems using DPc alone and $AlPcS_{2a}$ as shown in Table I.

To achieve a systemic PCI-mediated gene delivery utilizing micellar nanocarriers, polymeric micelles are required to accumulate in the target tissues and be taken up by the target cells, of which processes are known to occur in a time-dependent manner. On the other hand, the timing of the photoirradiation may be a critical factor in the PCI-mediated transfection (Prasmickaite et al. 2001). Hence, the effect of the photoirradiation timing on the photochemical transfection was then investigated. First, the effect of the prolonged incubation before photoirradiation was examined: after a 24 h continuous incubation with the combination of the pDNA- and DPc-incorporated micelles, HeLa cells were subjected to the medium replacement, followed by photoirradiation at the fluence of 5.4 J/cm^2. The transfection efficacy was evaluated after a further 48 h of post-incubation. As seen in Figure 9, an approximately 50-fold photochemical enhancement in the gene expression while

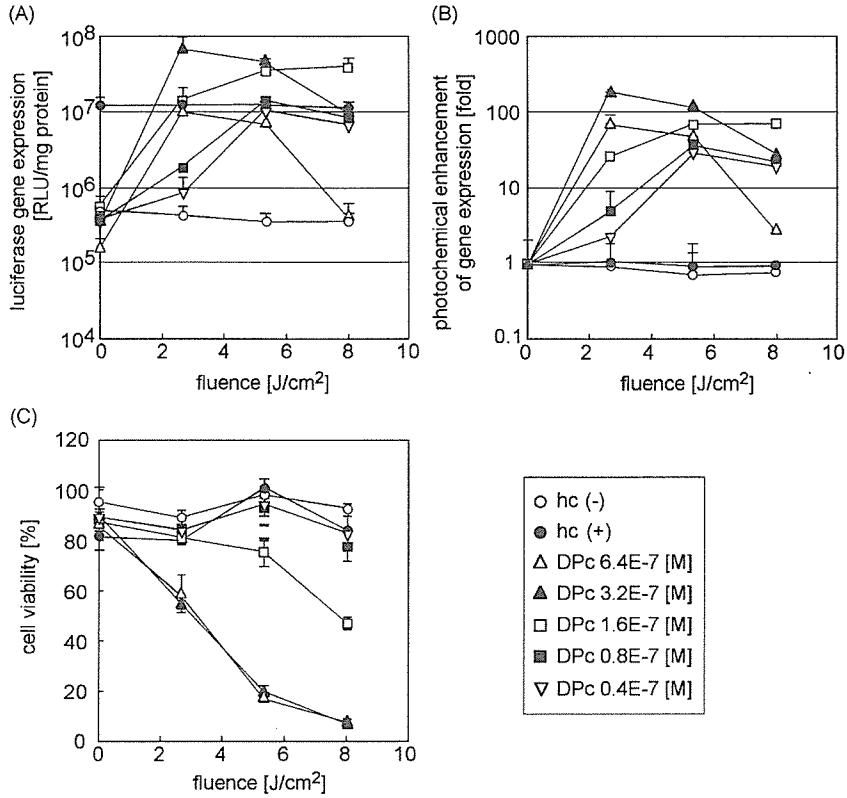

Figure 7. The effects on the DPc concentration and fluence on the transfection efficiency (A), photochemical enhancement of the gene expression (B) and photocytotoxicity (C) in the PCI-mediated transfection using DPc alone. The light irradiation was performed 6 h after incubation with the pDNA-incorporated micelles and free DPc, followed by 48 h post-incubation in a fresh medium.

maintaining more than an 80% cell viability was obtained under this condition, which appears to be consistent with Figure 5. Thus, the PCI using the DPc-incorporated micelles might be effective even after a prolonged incubation before photoirradiation. Note that the transfection efficiencies of the polyplex micelles under both irradiated and non-irradiated conditions decreased as the DPc concentration increased (Figure 9(A)), which may be due to the decreased cellular uptake of the polyplex micelles and/or interaction between the pDNA- and DPc-incorporated micelles as discussed above. In a second set of experiments, a certain lag time was placed before the photoirradiation of the HeLa cells in freshly replaced medium after a 6 h incubation with the combinational formulation of pDNA- and DPc-incorporated micelles. The transfection efficacy was evaluated 48 h after the photoirradiation (5.4 J/cm^2). As shown in Figure 10, post-incubation in the micelle-free medium after the 6 h treatment with the combinational micellar formulation resulted in a time-dependent decrease in the efficacy of the PCI-mediated transfection. This result seems to be consistent with the previous observation by Prasmickaite et al. (2001) suggesting that, in the PCI-mediated transfection, gene carriers may need to be translocated into the cytosol before their movement from the endosome to the lysosome. Therefore, to achieve a successful *in vivo* PCI-mediated gene delivery, the timing of the photoirradiation should be optimized in consideration of the balance between the effective accumulation of gene carriers as well as photosensitizers in the target cells and the prompt photo-induced translocation of gene carriers from the endosome to the cytosol before their movement to the lysosome.

The PCI is a smart concept, which can be basically used for the site-directed transfection in a light-inducible manner. In previous studies, $AlPcS_{2a}$ was demonstrated to be effective in the PCI (Høgset et al. 2002, 2004); however, the photochemical enhancement of the transfection was accompanied by the photocytotoxicity (Høgset et al. 2000). Although $AlPcS_{2a}$ is known to be internalized by the endocytic pathway, it is likely that $AlPcS_{2a}$ may interact with the plasma membrane to some extent as well as relocalize to some cytoplasmic organelles such as the mitochondria and endoplasmic reticulum during the photoirradiation, thereby inducing the inevitable photocytotoxicity (Moan et al. 1994; Macdonald and Dougherty 2001). Hence, considerable efforts have been devoted to the optimization of the experimental conditions for reducing the photocytotoxicity in the PCI-mediated transfection (Høgset et al. 2000). Also, the delivery of photosensitizers to the target cell should be taken into consideration in order to accomplish the *in vivo* PCI-mediated gene delivery.

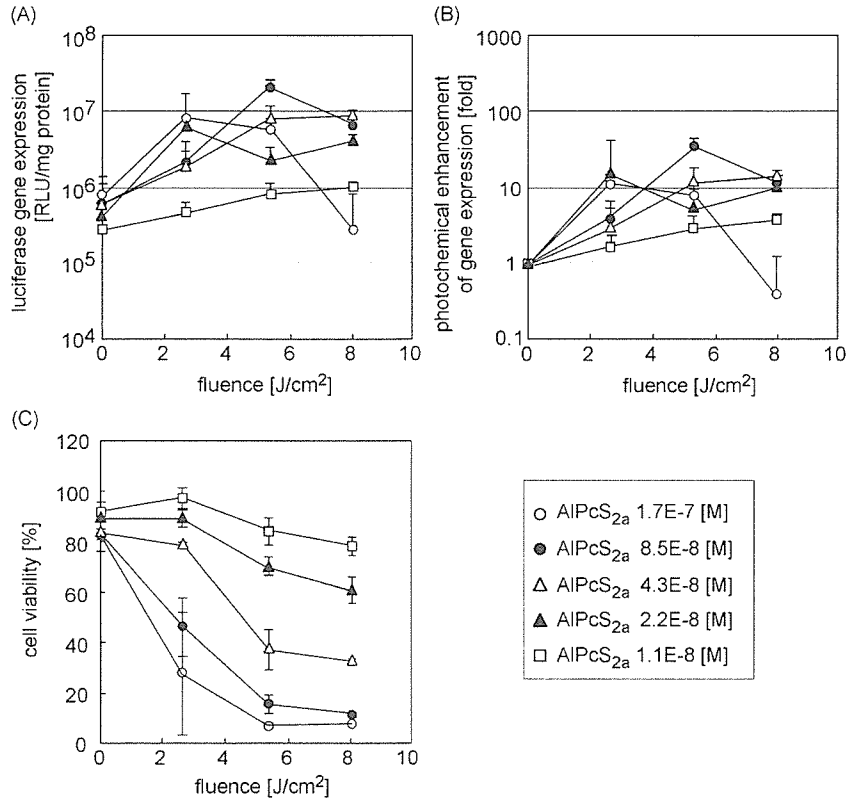

Figure 8. The effects on the $AlPcS_{2a}$ concentration and fluence on the transfection efficiency (A), photochemical enhancement of the gene expression (B) and photocytotoxicity (C) in the PCI-mediated transfection using $AlPcS_{2a}$. The light irradiation was performed 6 h after incubation with the pDNA-incorporated micelles and $AlPcS_{2a}$, followed by 48 h post-incubation in a fresh medium.

In this regard, we have recently developed DPc as a new photosensitizer for the PCI (Nishiyama et al. 2005). It has been demonstrated that the anionic DPc might electrostatically interact with the surface of the cationic polyplex to form the ternary complex enveloped with DPc, thus giving the same internalization and subcellular localization between DPc and the polyplex. Meanwhile, DPc exhibited a pH-dependent membrane binding ability, allowing the selective photodamaging of the endosomal membrane. Consequently, the ternary complex showed more than 100-fold photochemical enhancement of the gene expression with reduced photocytotoxicity on the cultured cells and *in vivo* light-selective gene transfer to the conjunctival tissues in rat eyes (Nishiyama et al. 2005). Thus, it was suggested that the design of the ternary complex might be effective for the PCI-mediated gene delivery; however, the ternary complex system is unlikely to be used for the systemic delivery. It is known that highly negatively-charged macromolecules can be excluded from the blood circulation due to the hepatic uptake by scavenger receptors of the non-parenchymal cells (Takakura and Hashida 1996).

In this study, the combinational formulation of the pDNA- and DPc-incorporated micelles was used in the PCI-mediated transfection. Polymeric micelles, of which the drug-loaded core is covered with a dense and hydrophilic PEG palisade, are characterized by their small size (less than 100 nm), excellent biocompatibility and stability in biological media (Kataoka et al. 1993, 2001; Nishiyama and Kataoka, 2006). We have so far demonstrated that polymeric micelles incorporating antitumor drugs can stably circulate in the bloodstream and effectively accumulate in solid tumors (Kwon et al. 1994; Nishiyama et al. 2003; Bae et al. 2005). Accordingly, in this study, we have used polymeric micelles as nanocarriers for the pDNA and DPc delivery, expecting their future application in systemic administration. In particular, this paper focused on demonstrating the feasibility of our strategy using the combinational formulation of the pDNA- and DPc-incorporated micelles in the PCI-mediated transfection *in vitro*. In this strategy, both polymeric micelles are assumed to be taken up by the cell through the endocytic pathway and show the same subcellular localization, allowing selective photochemical damaging of the endosomal membrane and effective cytoplasmic delivery of the pDNA-incorporated micelles upon photoirradiation, which might be a key to the successful PCI-mediated transfection. Indeed, the PCI using the DPc-incorporated micelles achieved more than 200-fold photochemical enhancement of the gene transfection of the polyplex micelles. Importantly, the PCI using the combinational micellar formulation achieved a wide range of safe DPc

Table I. Photochemical enhancement of the gene expression and cell viability in the PCI-mediated transfection using each photosensitizer (fluence: 5.4 J/cm^2).

DPc-loaded micelle	DPc conc. (μM)	0.64	0.32	0.16	0.08
	(a) Photochemical enhancement (fold)	72.6 ± 30	211 ± 150*	123 ± 58***	55.7 ± 25
	(b) Cell viability (%)	50.7 ± 1.9	73.8 ± 6.4**	81.2 ± 4.8	86.1 ± 11
DPc	DPc conc. (μM)	0.64	0.32	0.16	0.08
	(a) Photochemical enhancement (fold)	47.1 ± 20	117 ± 16**	64.3 ± 13***	34.2 ± 4.5
	(b) Cell viability (%)	15.7 ± 2.0	18.0 ± 2.3**	73.8 ± 5.8	92.0 ± 4.0
$AlPcS_{2a}$	$AlPcS_{2a}$ conc. (μM)	0.17	0.085	0.043	0.022
	(a) Photochemical enhancement (fold)	8.09 ± 8.9	35.5 ± 8.9*, **	12.9 ± 6.0***	5.63 ± 2.8
	(b) Cell viability (%)	7.15 ± 1.0	15.9 ± 3.7**	37.8 ± 7.8	71.4 ± 3.8

*$P > 0.05$; **$P < 0.01$; and ***$P < 0.05$ ($n = 4$, unpaired t-test).

concentrations and light doses, in which remarkable enhancement of the transfection was achieved without a significant decrease in the cell viability. Such expanded ranges of safe DPc concentrations and light doses should be favorable for the *in vivo* PCI-mediated gene delivery.

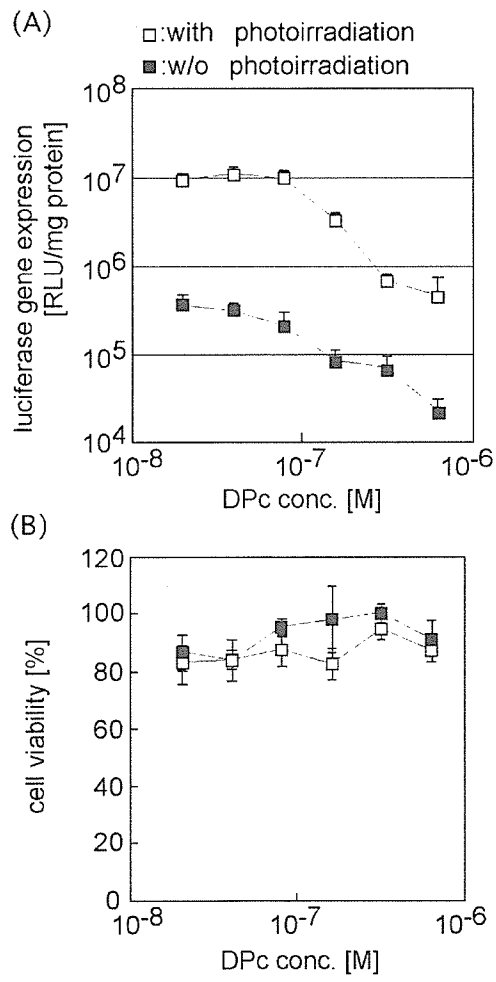

Figure 9. The transfection efficiency (A) and photocytotoxicity (B) in the PCI-mediated transfection using the DPc-incorporated micelles. The light irradiation (fluence: 5.4 J/cm^2) was performed after prolonged incubation (i.e. 24 h) with the pDNA- and DPc-incorporated micelles, followed by 48 h post-incubation in a fresh medium.

In conclusion, polymeric micelles might be a useful nanocarrier, which has been demonstrated to show prolonged blood circulation and thereby accumulate in the target tissues after intravenous administration, motivating us to study the PCI-mediated transfection using the combinational formulation of the pDNA- and DPc-incorporated micelles. Indeed, the PCI using the combinational micellar formulation achieved a remarkable photochemical enhancement of the transgene expression while maintaining an approximately 80% cell viability over a wide range of DPc concentrations and light doses. Thus, the usefulness of our strategy for *in vitro* trasnfection was successfully demonstrated. This system can be potentially useful for the gene therapy of solid tumors and ophthalmic diseases such as age-related macular regeneration (AMD) (Ideta et al. 2005). In addition to therapeutic genes, small interfering RNA (siRNA), which is known as the most powerful tool for sequence-specific silencing of the target genes (Elbashir et al. 2001), might also be delivered in a light-inducible manner by this strategy. The target-selective delivery of the therapeutic genes and siRNA

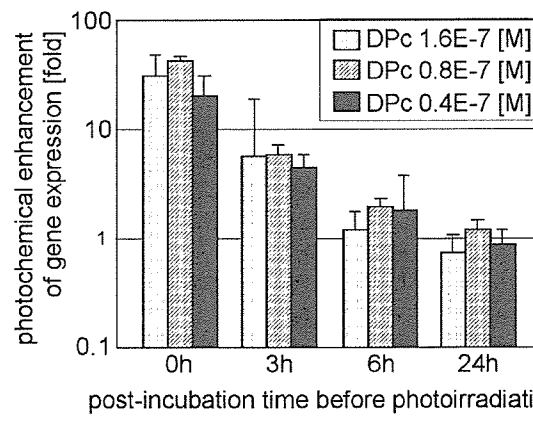

Figure 10. The effect of post-incubation time in the micelle-free medium before photoirradidation on the photochemical enhancement of the transfection of the polyplex micelles in the PCI-mediated transfection using the DPc-incorporated micelles. The cells were photoirradiated (5.4 J/cm^2) at defined post-incubation time after 6 h incubation with the pDNA- and DPc-incorporated micelles and medium replacement with a fresh one, followed by 48 h post-incubation.